Materials Horizons

ROYAL SOCIETY OF CHEMISTRY

REVIEW

View Article Online
View Journal | View Issue

Cite this: *Mater. Horiz.*, 2024, **11**, 1126

Strategies for utilizing covalent organic frameworks as host materials for the integration and delivery of bioactives

Lulu He,[abc] Le Wang,[ac] Zhen He,[a] Cheng Heng Pang,*[b] Bencan Tang,*[b] Aiguo Wu*[ac] and Juan Li*[ac]

Received 17th September 2023,
Accepted 1st December 2023

DOI: 10.1039/d3mh01492d

rsc.li/materials-horizons

Covalent organic frameworks (COFs), a new and developing class of porous framework materials, are considered a type of promising carrier for the integration and delivery of bioactives, which have diverse fascinating merits, such as a large specific surface area, designable and specific porosity, stable and orderly framework structure, and various active sites. However, owing to the significant differences among bioactives (including drugs, proteins, nucleic acid, and exosomes), such as size, structure, and physicochemical properties, the interaction between COFs and bioactives also varies. In this review, we firstly summarize three strategies for the construction of single or hybrid COF-based matrices for the delivery of cargos, including encapsulation, covalent binding, and coordination bonding. Besides, their smart response release behaviors are also categorized. Subsequently, the applications of cargo@COF biocomposites in biomedicine are comprehensively summarized, including tumor therapy, central nervous system (CNS) modulation, biomarker analysis, bioimaging, and anti-bacterial therapy. Finally, the challenges and opportunities in this field are briefly discussed.

Wider impact

Covalent organic frameworks (COFs) have received increasing attention owing to their potential applications in tumor therapy, central nervous system (CNS) modulation, biomarker analysis, bioimaging, and anti-bacterial therapy. More importantly, COFs with a high porosity, abundant active sites, and stimulus-responsive structures, usually function as host materials for the integration and delivery of bioactives in the above-mentioned practical applications. In this review, we summarize and discuss three types of synthetic strategies for the preparation of COF-based host–guest systems towards diverse bioactives, including small molecules, proteins, nucleic acids and exosomes. In addition, the recent advances in various types of COFs towards diverse biomedical applications are discussed in detail. This review also provides a complete overview of the current developments in COF-based nanosystems from the viewpoint of host–guest connection approach design and synthetic strategies, and their applicability in biomedical applications. We believe that the integration approaches of COFs and bioactives elucidated in this review will provide a significant basis for exploring next-generation COF-based integrated nanosystems.

1. Introduction

Covalent organic frameworks (COFs) are a class of porous crystalline organic polymers formed by covalent bonding with light elements (C, H, O, N, and B), which can be precisely regulated in terms of structure type through reversible condensation reactions to construct preferred topologies based on the connectivity and shape of the monomer building blocks.[1–4] With the progression of host–guest chemistry, several functional COFs have been synthesized to entrap specific bioactives (guests) in their skeletons (hosts), producing structurally stable host–guest ensembles (termed cargo@COF). Thus far, host–guest systems for bioactives based on COFs have been much less explored compared to those based on traditional carriers (mesoporous silica,

[a] *Ningbo Key Laboratory of Biomedical Imaging Probe Materials and Technology, Zhejiang International Cooperation Base of Biomedical Materials Technology and Application, Chinese Academy of Sciences (CAS) Key Laboratory of Magnetic Materials and Devices, Ningbo Cixi Institute of Biomedical Engineering, Zhejiang Engineering Research Center for Biomedical Materials, Ningbo Institute of Materials Technology and Engineering, Chinese Academy of Sciences, Ningbo, 315201, China. E-mail: aiguo@nimte.ac.cn, lij@nimte.ac.cn*

[b] *Department of Chemical and Environment Engineering, The University of Nottingham Ningbo China, Ningbo, 315100, China. E-mail: Chengheng.Pang@nottingham.edu.cn, Bencan.Tang@nottingham.edu.cn*

[c] *Advanced Energy Science and Technology Guangdong Laboratory, Huizhou, 516000, China*

liposomes, chitosan, and others) or relatively novel vehicles (MOF, erythrocytes, exosomes, and others).[5–7]

Here, bioactives not only refer to small molecules, such as therapeutic drugs, but also biomacromolecules, including proteins and nucleic acids, and even more complex vesicles, such as exosomes. Bioactives alone often fail to achieve a satisfactory therapeutic result owing to their inherent drawbacks. For example, conventional chemotherapeutic drugs are always limited by poor targeting ability and serious side effects.[8] Furthermore, maintaining the activity of proteins and prolonging the half-life of nucleic acids *in vivo* are also some of the challenging issues.[9] However, owing to the unique properties of COFs, they can overcome these difficulties, and thus have attracted extensive attention for the integration and delivery of bioactives.

The main advantages of COFs as carriers for the integration of bioactives are as follows: (1) diverse COF-based functional materials with different sizes, topologies, morphologies, and physical/chemical properties that can be designed and fabricated using available organic linkers and linkages, which can be summarized in one word: designability. (2) COFs with a high crystallinity tend to provide an extremely high specific surface area (over 1000 $m^2 g^{-1}$), uniform pore shape, ultrahigh porosity, and adjustable and wide pore size distribution (from micropore to mesopore), making them an excellent host matrix for encapsulating bioactives. (3) COFs possess a good biocompatibility and low cytotoxicity, which is attributed to their organic and metal-free nature. (4) Through the post-synthetic modification (PSM) strategy, bonding defect functionalization (BDF) strategy, or other surface decoration approach, target molecules can be covalently attached to the COF backbone by reacting with the active sites of its linkers, while retaining the original framework. (5) Smart stimuli-responsive COFs have been successfully designed for controlled and sustained drug release due to the

Lulu He

Lulu He is currently a PhD student jointly trained at the University of Nottingham Ningbo China (UNNC) and the Ningbo Institute of Materials Technology and Engineering, Chinese Academy of Sciences (CNITECH). She received her Master's degree in Analytical Chemistry from the Zhejiang University of Technology in 2020. Currently, she is working on the design and preparation of nanoscale COFs for various biomedical applications.

Le Wang

Le Wang is currently a Master's student jointly trained at the Wenzhou Medical University (WMU) and CNITECH. She received her BS degree in Pharmaceutical Engineering from Southwest Jiaotong University in 2020. Her research interests include the synthesis of COF-based nanomaterials and their biomedical applications.

Cheng Heng Pang

Dr Cheng Heng Pang received his BS degree in Engineering from University of Nottingham, Semenyih, Selangor, Malaysia in 2008 and his PhD from University of Nottingham, Nottingham, Nottinghamshire, GB in 2012. Dr Pang is now a professor of Chemical Engineering and Advanced Materials, the director of Teaching and Learning, Deputy Head of Department (CEE), and the head of Research Group (AEEMT) of UNNC. Dr Pang's research interest, experience, and expertise are primarily focused on renewable energy and manufacturing of advanced materials for biomedical applications, particularly in anti-cancer therapy.

Bencan Tang

Bencan Tang received her BS and a MS degrees from Lanzhou University, and obtained a PhD degree from the University of Nottingham, UK, working on the biomimetic syntheses of complex polycyclic diterpenes found in corals. After postdoctoral work with Prof. David Harrowven at the University of Southampton, she joined Professor Paton's group at the University of Oxford to focus on computational studies of biomimetic syntheses of natural products. In 2014, Bencan became an Assistant Professor and in 2019, an Associate Professor at the University of Nottingham Ningbo China, where she explores the biomimetic syntheses of marine natural products, both computationally and experimentally. Her other research interests include artificial intelligence assisted drug discovery and organic photovoltaics.

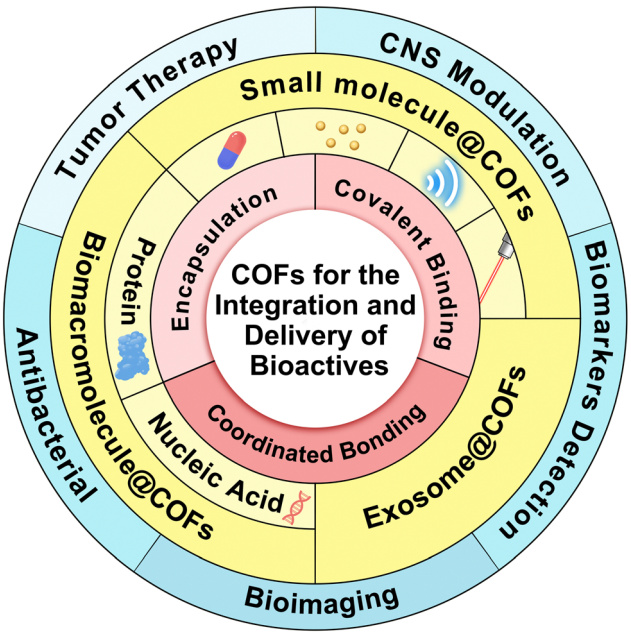

Scheme 1 Categorization of COFs as host materials for the integration and delivery of bioactives and their biomedical applications.

physical and chemical difference in the microenvironment between healthy and diseased tissues.

This review focuses on the integration strategies for cargo@COF complexes and their diverse biomedical applications (Scheme 1). Thus far, several excellent reviews have discussed COFs and their wide applications, such as catalysis,[10–12] gas storage and separation,[13,14] vapor sorption,[15] electronic and ionic conduction.[16–18] However, only a few further presented the diverse bio-applications of COFs.[19–21] Also, another limitation of existing reviews on COF-based carrier systems in the biomedical field is that almost all focused on cancer therapy, while ignoring other applications.[22] Thus, in this review, we highlight the importance of COFs as host materials for the delivery of bioactives and their applications, not only in cancer therapy but also in other biomedical fields. Notably, the use of COFs as hosts for the integration and delivery of bioactives is still in its infancy, making it important to summarize and introduce this COF-based specific area, expanding the applications of COFs.

2. Synthetic strategies for COF-based host–guest systems

To date, several reviews have summarized the processes for the synthesis of COFs including solvothermal,[23–25] ionothermal,[26,27] microwave-assisted,[28] sonochemical,[29,30] room-temperature,[31–33] mechanochemical,[34,35] electrochemical,[36] and light-promoted methods.[37] Alternatively, in this section, we focus on the synthetic strategies for the whole host–guest platform, denoted as cargo@COF, and present a brief review and summary. The currently reported synthetic strategies for the construction of cargo@COF complexes can be divided into three different paths, including (A) encapsulation, (B) covalent binding and (C) coordination bonding, as shown in Fig. 1, which will be discussed in detail in this section. Besides, Table 1 summarizes the diversity of cargo@COF delivery systems for various biomedical applications.

2.1 Encapsulation routes for COF-based system

The encapsulation method is a frequently used strategy to prepare host–guest systems. Specifically, the guest molecules are gradually allowed to enter the host materials until achieving adsorption and diffusion equilibrium with the help of electrostatic attraction, hydrogen bonding, van der Waals interactions, π interactions, and hydrophobic/hydrophilic effect. In recent years, numerous COFs have been successively used to accommodate cargos based on the encapsulation strategy.

Aiguo Wu

Dr Aiguo Wu received his BS degree from Nanchang University in 1998 and his PhD from Changchun Institute of Applied Chemistry, Chinese Academy of Sciences in 2003. After his postdoctoral studies at the University of Marburg, Marburg, Germany (2004 to 2005) and the California Institute of Technology, Pasadena, CA, USA (2005 to 2006), he moved to Northwestern University, Chicago, IL, USA as a Research Associate from 2006 to 2009. He is a professor at the CNITECH since 2009. Dr Wu's research area is primarily focused on the application of nanomaterials in biomedical, bioanalytical chemistry, and environmental sciences.

Juan Li

Dr Juan Li received her BS and MS degrees from Shenyang Pharmaceutical University in 2004 and 2007, respectively. She received her PhD from the Department of Physiology of Cognitive Processes, Max Planck Institute for Biological Cybernetics and the University of Tubingen, Germany in 2012. After that, she worked as a postdoctoral researcher in CNITECH from 2012 to 2014. Dr Li is now a professor at the CNITECH since 2020. Her research includes the design and application of neuropeptide-based nanomaterials for the imaging and therapy of tumors as well as central nervous system diseases.

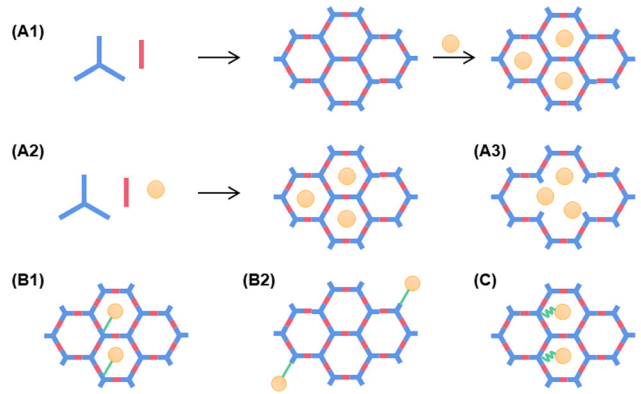

Fig. 1 The synthetic strategies for the construction of cargo@COF. (A1) Two-step encapsulation procedure. (A2) One-pot encapsulation method. (A3) Hollow encapsulation process. (B1) Post-synthetic modification (PSM). (B2) Bonding defect functionalization (BDF). (C) Coordination bonding strategy. The blue and red graphics represent monomers, the yellow balls represent cargos (including small molecules, biomacromolecules and exosomes), the green straight lines stand for covalent bonds, and the green curves stand for coordination bonds.

2.1.1 The two-step encapsulation procedure. The two-step encapsulation procedure is commonly used for the preparation of cargo@COF systems by immersing the prepared COF carriers in cargo-containing solutions with continuous stirring. In step I, it is critical to construct COF-based carriers with outstanding characteristics that satisfy the delivery conditions, such as large surface area, tunable pore size, and ordered channels. In step II, the cargos are inserted in the pre-synthesized COFs with good stability and dispersibility under long-time stirring until adsorption and diffusion balance is reached for the cargo molecules and COF carriers. Usually, it takes a few of hours to construct cargo@COF composite systems.

For example, a three-dimensional (3D) COF (TUS-84) with ***scu-c*** topology was synthesized *via* the [8+4] imine condensation reaction in 2022.[38] This is a typical example of a COF synthesized through the traditional solvothermal method, where two monomers (DPTB-Me and TAPP), catalyst (6 M aqueous acetic acid) and solvent (mesitylene and 1,4-dioxane, 5 : 5, v/v) are mixed at 120 °C for 3 days. As shown in Fig. 2(A), the PXRD and HRTEM characterization results of TUS-84 indicated it had an ordered microporous structure with high crystallinity, which showed great potential for drug delivery. Subsequently, in the second step of drug loading, the TUS-84 powder was immersed in a hexane solution of ibuprofen, and then stirred at room temperature for 4 h. Both UV-Vis spectroscopy and thermogravimetric analysis (TGA) were conducted to measure the loading capacity of ibuprofen in Ibu@COF, and the results from these two methods corresponded well, revealing a value of 11 wt%. Similarly, Sabuj Kanti Das and co-workers employed a novel biocompatible COF (TRIPTA-COF) to serve as a great nanocarrier for cisplatin (Fig. 2(B)).[39] Briefly, the monomers were added to a dry Pyrex tube, followed by the addition of the solvent and catalyst. Subsequently, the homogeneously dispersed reaction mixture was degassed by three freeze–pump–thaw cycles, flame-sealed, and then allowed it to react for 4 days. Finally, cisplatin was impregnated in the unoccupied pores of the COF by overnight stirring using DMSO as the solvent. The quantitative drug loading assay was performed by TGA and ICP-OES techniques, resulting in a high loading efficiency of 31.19%.

Unlike traditional solvothermal COF synthesis, room temperature synthesis approaches do not require any rigorous reaction conditions, such as high temperature, long reaction time and inert atmosphere (absence of water and oxygen). Alternatively, mild reaction conditions are employed to construct cargo@COF systems. In 2023, Han *et al.* synthesized a dual-drug delivery system to immobilize both the photosensitizer indocyanine green (ICG) and the hypoxia-activated prodrug AQ4N.[40] In a typical synthesis procedure, a transparent homogeneous solution of monomers and catalyst was stirred for 12 h at room temperature. Subsequently, the residue was collected by centrifugation, followed by washing with anhydrous ethanol three times. The pre-synthesized TPB-DMTP-COF was used to entrap ICG and AQ4N stepwise through stirring for 12 h to obtain COF@ICG and COF@ICG/AQ4N, respectively. As shown in Fig. 3(A), the TEM images verified that all products were dispersed uniformly.

In almost all previous studies, COFs were synthesized on the milligram-scale; however, Dong's group proposed a novel strategy that expanded the synthesis procedure to the gram-scale, while maintaining the particle size and spherical morphology.[41] The photocatalytic cascade reactions played a dominant role in the newly propounded strategy, which were performed to prepare four previously reported imine-linked COFs after sequential reactions under ambient conditions at room temperature (Fig. 3(B)). Subsequently, RT-COF-1 with an average size of 167.9 nm was selected as a model nanocarrier for the delivery of the anticancer drug lonidamine (LND). As shown in Fig. 3(B)-III, the LND@ RT-COF-1 composite was simply obtained by immersing RT-COF-1 in an ethanol solution of LND for 24 h.

2.1.2 The one-pot encapsulation method. Moreover, another encapsulation method is defined as the "one-pot" encapsulation procedure, where all the necessary reactants including the monomers, drugs, and catalyst are added to "one pot" for the fabrication of the drug@COF system. Compared with the general two-step process, the "one-pot" method is more convenient and time-saving. For example, in 2019, DOX was successfully *in situ* loaded in a COF *via* a one-pot method for the first time by Liu and co-workers.[42] Specifically, the raw materials were mixed, followed by stirring at room temperature for 24 h. Finally, as shown in Fig. 4(A), the DOX@COF platform with a high drug loading capacity of 32.1 wt% was successfully constructed.

Recently, Zou *et al.* fabricated a CUR@COF nanosystem *via* a facile "one pot" method for the delivery of curcumin (CUR).[43] The CUR loading capacity in the COF was calculated to be in the range of 15.05% to 27.68% with an increase in the content of CUR from 2 to 8 mg, while the encapsulation efficiency decreased from 78.26% to 49.63%. Furthermore, the standard CCK-8 assay was conducted to evaluate the *in vitro* cytotoxicity of COF or CUR@COF, and the results showed that 91% and 95% cells survived at the concentration of 200 μg mL^{-1}, indicating the low cytotoxicity and good biocompatibility of COF and CUR@COF (Fig. 4(B)).

Table 1 Summary of cargo@COF integration and delivery systems for biomedical applications

Year	Carrier	Cargo	Composite strategy	Loading percentage	Applications	Ref.
2015	PI-COF-4	IBU/captopril/caffeine	Two-step encapsulation	~20 wt% for IBU	—	55
	PI-COF-5					
2016	PI-3-COF	5-FU/captopril/IBU	Two-step encapsulation	16 wt%	Drug delivery *in vitro*	56
	PI-2-COF			30 wt%		
2017	PCTF	IBU	Two-step encapsulation	19 wt%	—	57
	PCTF-Mn			23 wt%		
2017	TpAPH	5-FU	PSM	12 wt%	Targeted drug delivery	48
	TpASH					
2018	APTES-COF-1	DOX	Two-step encapsulation	9.71 ± 0.13 wt%	Chemotherapy	58
2019	TPB-DMTP-COF	Por	BDF	0.091 ± 0.010 μmol mg^{-1}	PDT/PTT	59
		VONc	Two-step encapsulation	0.256 ± 0.030 μmol mg^{-1}		
2019	COF-LZU1	BODIPY-2H	BDF	0.1545 ± 0.0220 mmol g^{-1}	PDT	50
		BODIPY-2I		0.1360 ± 0.0312 mmol g^{-1}		
2019	TAPB-DMTP-COF	DOX	One-pot encapsulation	32.1 wt%	Chemotherapy	42
2019	PI-CTF	Sorafenib	Two-step encapsulation	83 wt%	Anti-cancer *in vitro*	60
2019	TP-Por-COF	CAD/IR783	Two-step encapsulation	—	CT/PTT	61
2020	DT-COF	Carboplatin	Two-step encapsulation	31.32 wt%	—	62
2020	TPB-DHTP-COF	5-FU	Two-step encapsulation	44 μg mg^{-1}	Chemotherapy	63
	COF-HQ		PSM	73 μg mg^{-1}		
2020	SS-COF	DOX	Two-step encapsulation	36 wt%	Chemotherapy	64
	F68@SS-COF			21 wt%		
2020	TPA-TA-BD-COF	DOX	Two-step encapsulation	35 wt%	Anti-cancer *in vitro*	65
2020	HY/SS COF	DOX	Two-step encapsulation	18 wt%	—	66
2020	$COF_{TTA\text{-}DHTA}$	Pirfenidone	Two-step encapsulation	32 ± 4 wt%	PDT	67
2021	Tph-Dha-COF	Fe	Covalent binding	1.6 mg mg^{-1}	Chemotherapy/CDT	52
		DOX	Two-step encapsulation			
2021	TA-COF	Ce 6	Two-step	14.3 wt%	Chemotherapy/PDT	68
		TPZ	encapsulation	17.8 wt%		
2021	Tph-Dha-COF	Gambogic acid	Two-step encapsulation	0.004 μg $μg^{-1}$	PTT	69
2021	Tf-TAPB-COF	FcCHO	Two-step encapsulation	0.170 ± 0.018 μmol mg^{-1}	CDT	51
		RSL3		0.201 ± 0.032 μmol mg^{-1}		
2021	TCOF	DOX	Two-step encapsulation	~28.57%	Chemotherapy	70
2021	RT-COF-1	Lonidamine	Two-step encapsulation	0.66 ± 0.05 mmol g^{-1}	Chemotherapy	41
2021	JUC-556 (*E*/*Z*)	Cytarabine	Two-step encapsulation	—	—	71
2022	DMTP-TAPB-COF	Heteropoly blue	One-pot encapsulation	—	PTT	72
2022	JUC-580	Cisplatin	Two-step encapsulation	20 wt%	Cell fluorescence imaging	73
	JUC-581					
2022	COF-366	Plumbagin	Two-step encapsulation	16.3 wt%	Anti-cancer *in vitro*	74
2022	TAPB-DMTA-COF	Curcumin (CUR)	One-pot encapsulation	27.68 wt%	Wound dressing	43
2022	TRIPTA-COF	Cis	Two-step encapsulation	31.19%	Chemotherapy	39
2022	DF-TAPB-COF	5-FU	Two-step encapsulation	up to 60 wt%	—	75
	DF-TATB-COF	Captopril				
2022	TPE-ss COF	Matrine	Two-step encapsulation	15.61 ± 0.23 wt%	Myocardial ischemia/reperfusion injury	76
2022	$AQ4N@THPP_{TK}$-PEG	AQ4N	Two-step encapsulation	26.35 wt%	CT/PDT	77
2022	TAPP-ANT-COF	Cypate	Two-step encapsulation	11.2%	PDT/PTT	78
2022	PER@PDA-COF-1	Mitoxantrone	Two-step encapsulation	~63%	CT	79
2022	DiSe-Por	DOX	Two-step encapsulation	35.12%	CT/PTT/CDT	80
2022	COF-909	Cu	Coordinated bonding	10.76%	CDT/PDT/Immunotherapy	54
		Fe		10.05%		
		Ni		9.17%		

Table 1 (*continued*)

Year	Carrier	Cargo	Composite strategy	Loading percentage	Applications	Ref.
2022	TAPB-DMTP-COF	DOX Camptothecin	Two-step encapsulation	92 μg mg^{-1} 222 μg mg^{-1}	Tumor therapy	81
2022	APTES-COF-1	Rapamycin	Two-step encapsulation	—	Attenuate retinal ganglion cells death	82
2022	Hollow PDA-TMD-COF	Apatinib	Two-step/hollow encapsulation	~40.5 wt%	MWTT/CT	83
2022	TUS-84	IBU	Two-step encapsulation	11.05 wt%	—	38
2022	SP-COFs	$POCl_3$	Covalent binding	—	Inhibition of amyloid-β (Aβ) fibrillation	84
2023	TUS-64	Captopril/IBU/isoniazid/5-FU/brimonidine	Two-step encapsulation	4.09–17.37 wt%	—	85
2023	DSPP-COF	5-FU	Two-step encapsulation	~0.86 μmol mg^{-1}	Chemotherapy/PDT	86
2023	DMTP-TPB-COF	ICG/AQ4N	Two-step encapsulation	53.1% for ICG	PTT/PDT/chemotherapy	40
2023	Hollow HAPTP-TFPB/TPA/TFPA 2DCOFs	IBU	Two-step encapsulation	12–20 wt%	—	45
2023	TAPB-DMTP-COF	Rose Bengal (RB)	Two-step encapsulation	20.6%	SDT	87
2023	TAPB-DVA-COF	DOX/RB/CUR/ICG/Ce6	Hollow encapsulation	41.7–67.8%	SDT	47
2015	COF-DhaTab	Trypsin	Two-step encapsulation	15.5 μmol g^{-1}	—	88
2018	NKCOF-1	Lysozyme/tripeptide/lysine	Covalent binding	22 μmol g^{-1} for lysozyme	Chiral separation	89
2018	TPB-DMTP-COF	Amano lipase PS	Two-step encapsulation	0.95 mg mg^{-1}	—	90
2020	TPMM COF	α-amylase	Two-step encapsulation	550 mg g^{-1}	Biocatalyst	91
2020	Tph-Dha-COF	Survivin antisense strand	Two-step encapsulation	0.572 nmol mg^{-1}	Tumor imaging/PDT/prognostic evaluation	92
2020	TAPB-BTCA-COF	Ovalbumin	Two-step encapsulation	—	PTT/immunotherapy	93
2020	COF-1 COF-5	GOx/iunsulin	Two-step encapsulation	~45%	Anti-type 1 diabetes mellitus	94
2021	TTA-DFP-nCOF	Insulin	Two-step encapsulation	~65 wt%	Anti-type 1 diabetes mellitus	95
2021	DHA-TAPP-COF	GOx CAT	Two-step encapsulation	46.1 μg mg^{-1} 392.58 μg mg^{-1}	PDT/starvation therapy	96
2021	TPB-DMTP-COF	Survivin mRNA MUC1 aptamers	Two-step encapsulation	0.106 nmol mg^{-1} 0.120 nmol mg^{-1}	Biomarkers fluorescence imaging	97
2021	Tph-Dha-COF	DNA	Covalent binding	0.695 nmol mg^{-1}	Cancer cell imaging	98
2021	CTF-PEG-PEI	pDNA	Two-step encapsulation	—	Gene transfection	99
2022	COF-LZU1	Trypsin/HRP/GOx/BSA	One-pot encapsulation	5.0 mg g^{-1} for trypsin	—	44
2022	$[OH]_{x\%}$-TD-COFs	Cytochrome *c* (Cyt *c*)	Covalent binding	—	—	100
2022	BPTA-TPB-COF	Peptide/HRP	Covalent binding	—	Protein detection	101
2022	ETTA-TPAL-COF	Glucose oxidase GOD	Two-step encapsulation	30 μg mg^{-1}	Glucose detection	102
2022	Alkynyl-COF	DNA	Covalent binding	16 μg mg^{-1}	Exosomes detection	103
2023	Alkynyl-COF	DNA/HRP	Covalent binding	—	Exosomes analysis	104
2023	TAPB-DMTA-COF	Peptide T5/SOD/CAT	Covalent binding Two-step encapsulation	16.29 wt%	Modulates oxidative stress in Alzheimer's disease	105
2023	Tp-Bd-COF	Cyt *c*/GOx/HRP	Hollow encapsulation	57–127 mg g^{-1}	Glucose detection	106
2023	TAPB-DMTA COF	GOx/Cyt *c*	Two-step encapsulation	—	Biocatalyst	107
2022	TPB-DHTA-COF	Exosome	Two-step encapsulation	—	Diabetic fester wound healing	108

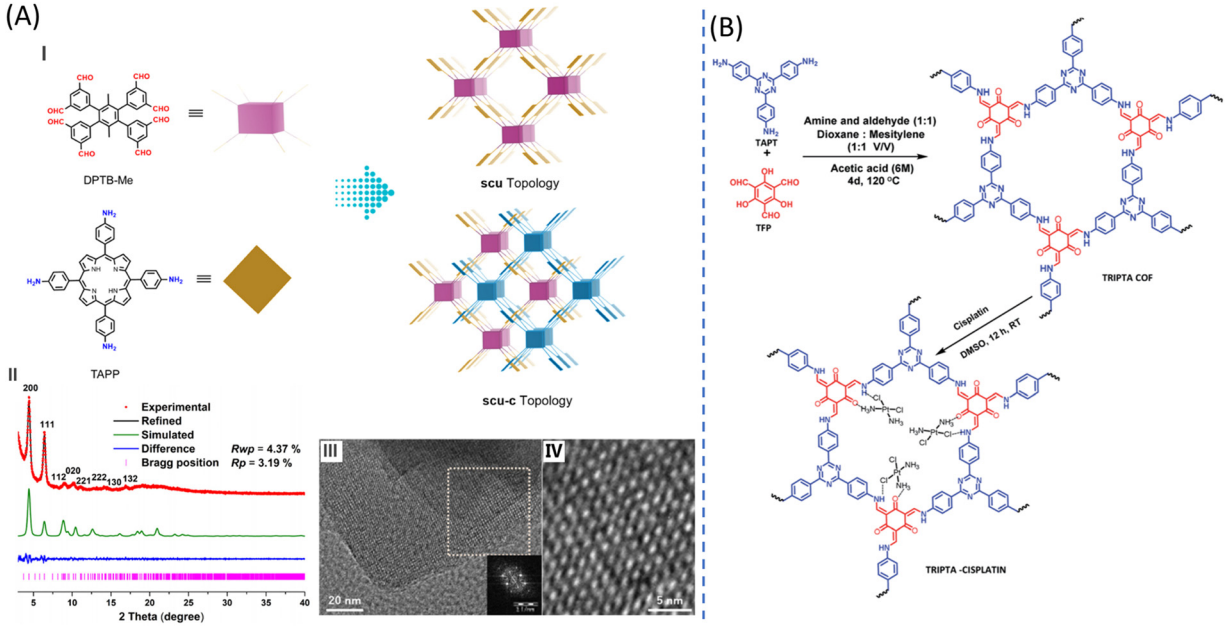

Fig. 2 The two-step encapsulation procedure *via* the solvothermal method. (A) I. Strategy for the constructing of 3D COFs with ***scu*** or ***scu-c*** topology. II. PXRD patterns and HRTEM images of TUS-84. Reproduced from ref. 38 with permission from ACS Applied Materials & Interfaces, Copyright 2022. (B) Synthesis of cisplatin-loaded TRIPTA-CISPLATIN. Reproduced from ref. 39 with permission from Nanoscale Advances, Copyright 2022.

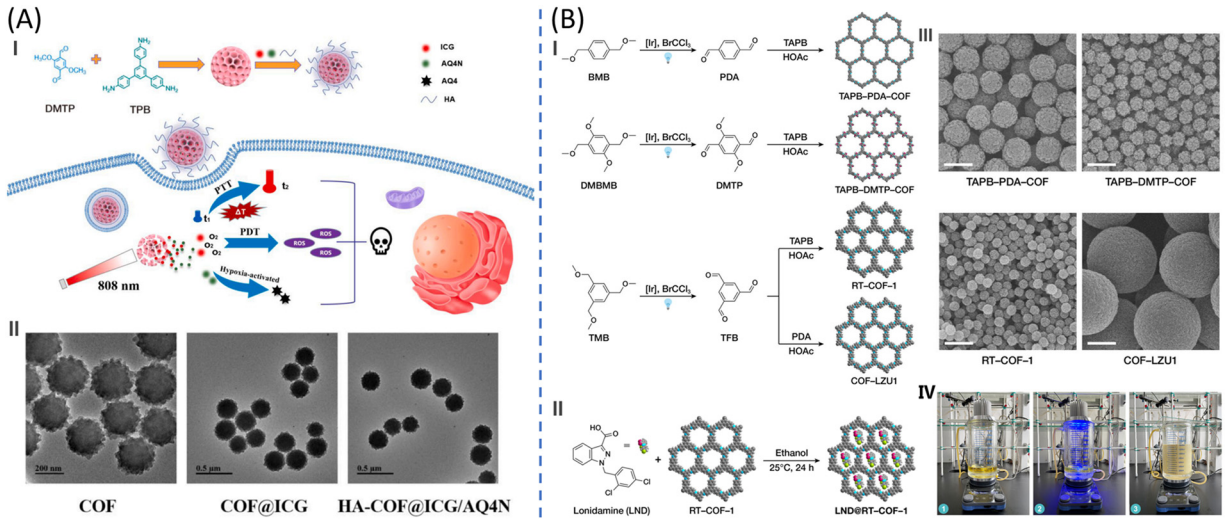

Fig. 3 The two-step encapsulation procedure with room temperature synthesis approach. (A) I. Synthesis process of HA-COF@ICG/AQ4N. II. TEM images of COF, COF@ICG, and HA-COF@ICG/AQ4N nanoparticles. Reproduced from ref. 40 with permission from Colloids and Surface B: biointerfaces, Copyright 2023. (B) I. Synthesis process of imine-linked COFs. II. SEM images of COFs and equipment for the gram-scale synthesis of RT-COF-1. III. Synthesis process of LND@RT-COF-1. Reproduced from ref. 41 with permission from Advanced Therapeutics, Copyright 2021.

The ''one-pot'' method was used for the delivery of not only small molecules but also for the immobilization of biomacromolecules, such as enzymes. Recently, a hollow COF-based capsule for the template-free *in situ* encapsulation of enzymes was prepared by Chao and co-workers.[44] As shown in Fig. 4(C), the enzyme (trypsin) and raw materials in process for the synthesis of COF-LZU1 (benzene-1,3,5-tricarbaldehyde and *p*-phenylenediamine) were mixed in 1,4-dioxane at room temperature and left to react for 3 days without stirring. Finally, the trypsin@COF-LZU1 composites were successfully prepared *via* the single-step and template-free process. With an increase in the content of trypsin from 0 to 6.0 mg, the crystallinity of COF-LZU1 showed no significant change given that the X-ray diffraction peaks of the products remained the same. More importantly, this single-step strategy can also be extended to other biomolecules (HRP, GOx and BSA), making it a high potential method for the encapsulation of biomacromolecules.

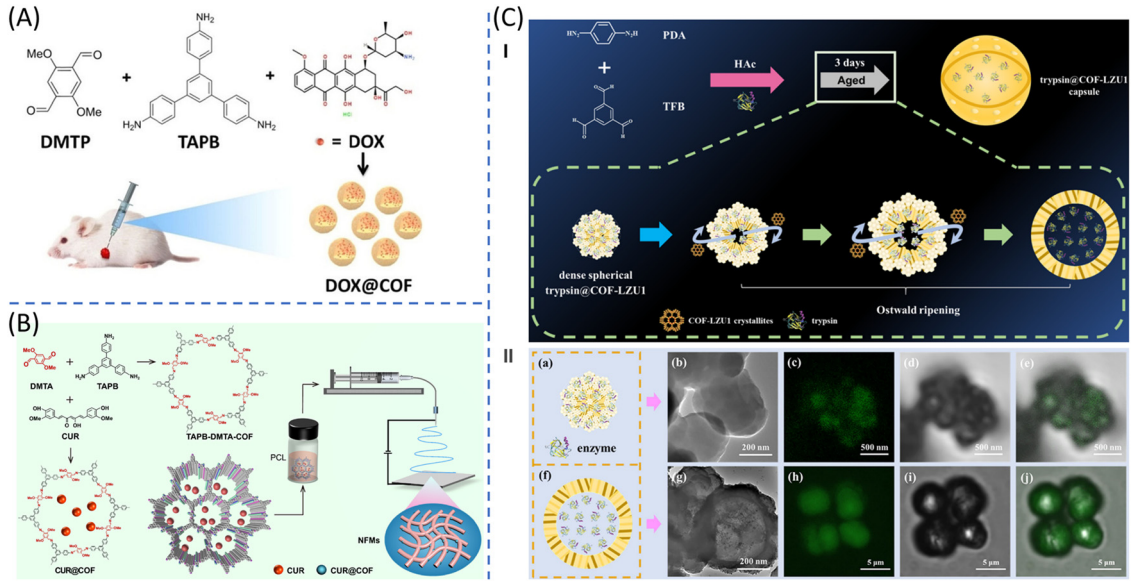

Fig. 4 The one-pot encapsulation method. (A) Illustration of the synthesis and application of DOX@COF. Reproduced from ref. 42 with permission from Chemistry, Copyright 2019. (B) A schematic diagram of the preparation of CUR@COF. Reproduced from ref. 43 with permission from ACS Applied Materials & Interfaces, Copyright 2022. (C) The synthesis process and formation mechanism of the trypsin@COF-LZU1 capsule. Reproduced from ref. 44 with permission from ACS Applied Materials & Interfaces, Copyright 2022.

2.1.3 The hollow encapsulation process. Hollow nanoparticles with empty cavities are fascinating materials for the immobilization and delivery of biomolecules. These hollow materials are usually fabricated *via* soft/hard templating routes, sacrificial template methods, *etc.*

Recently, Du and co-workers proposed a self-templating method for the synthesis of a hollow 2D COF using a newly synthesized building block (2,3,6,7,10,11-hexakis(4-aminophenyl) triphenylene, HAPTP) under solvothermal conditions.[45] Impressively, the newly synthesized COFs were homogeneous solid spheres initially; however, a transformation occurred based on a time-dependent model, gradually turning into uniform hollow spheres accompanied by the Ostwald ripening process, as shown in Fig. 5(A). Subsequently, IBU was loaded successfully, and the loading capacity was determined by TGA to be as high as 20 wt%, benefitting from the high crystallinity quality and large surface area of the host COFs.

Li *et al.* used metal–organic frameworks (MOFs) as sacrificial templates to construct COF capsules for the encapsulation of an enzyme (Fig. 5(B)).[46] Firstly, the catalase (CAT) molecules were *in situ* encapsulated in digestible MOFs to form biomacromolecules@MOF, which could protect enzymes from losing their bioactivities. Secondly, the COF coating was grown on the surface to obtain biomacromolecule@MOF@COF core–shell structures. Finally, the MOF core was etched and the as-obtained hollow COF was used to immobilize the enzyme successfully. Consequently, compared with free CAT or the CAT@MOF complex, the CAT@COF capsules exhibited an excellent protection effect on the enzyme activity under various perturbation conditions including acid, proteases, acetone and high temperature.

Liu and coworkers proposed a fascinating strategy for the controllable synthesis of a series of hollow COFs *via* the oxidation of the imine bond *via* hydroxyl radicals ($^{\bullet}OH$) generated from the Fenton reaction.[47] The whole procedure included two steps (Fig. 5(C)), where firstly, a solvent evaporation strategy was proposed for the synthesis of high crystallinity COFs, by which the solvent (ACN) and catalysis (acetic acid) were evaporated when exposed in an uncovered vessel at mild temperature (room temperature to 60 °C) with stirring. Secondly, the synthesized COFs were converted into hollow COFs by breaking the imine bond under the combined action of ferric chloride ($FeCl_3$), hydrogen peroxide (H_2O_2) and acetic acid. Whether in step one or two, several COFs or HCOFs with diverse morphologies were successfully achieved, demonstrating the universality of this strategies. Finally, the synthesized TAPB-DVA-HCOF functioned as a nanocarrier to load five small molecule drugs. The DLC was calculated to be in the range of 41.7% to 67.8% and EE calculated to be in the range of 31.5% to 75.1% for the five drugs, which were much higher than previous reports. Finally, Ce6@HCOF showed an excellent enhanced sonodynamic cancer therapy ability and anti-tumor efficiency both *in vitro* and *in vivo*.

2.2 Covalent binding strategy for COF-based system

The active sites, whether on the side chain of the monomers or unbonded functional groups, are always regarded as potential locations for the covalent binding of targeted cargos, which is defined as post-synthetic modification (PSM) for the former or bonding defect functionalization (BDF) for the latter.

The active sites of COFs can be connected with specific guest molecules through covalent bonds. For example, Shouvik Mitra *et al.* covalently connected folic acid (FA) to a COF (TpASH-FA) through three sequential post-synthetic modifications (Fig. 6(A)).[48] Firstly, the phenolic hydroxyl groups of the

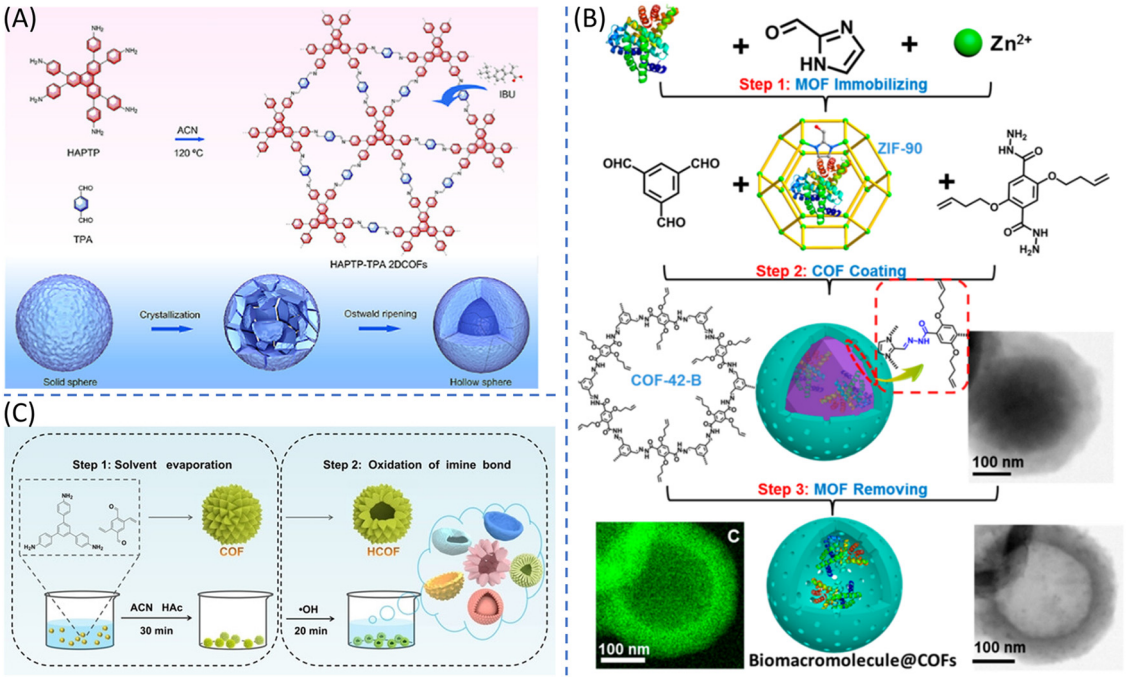

Fig. 5 The hollow encapsulation procedure. (A) I. Process for the synthesis of HAPTP-TPA 2DCOFs. Reproduced from ref. 45 with permission from Chemistry of Materials, Copyright 2023. (B) Synthetic route for biomacromolecule@COF capsules. Reproduced from ref. 46 with permission from Journal of the American Chemical Society, Copyright 2020. (C) Synthesis process of the COF and hollow COF. Reproduced from ref. 47 with permission from Angewandte Chemie-International Edition, Copyright 2023.

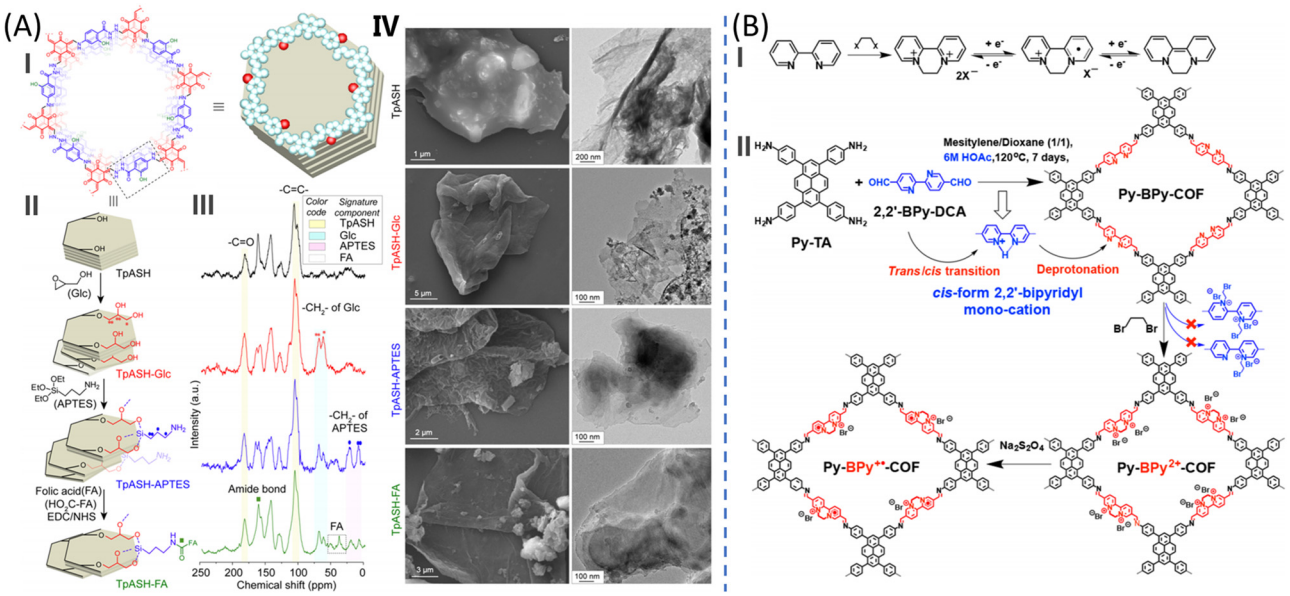

Fig. 6 Post-synthetic modification (PSM). (A) I. A schematic diagram of the chemical structure of COF nanosheets. II. Sequential PSM processes of TpASH to TpASH-FA and their NMR spectra (III), as well as SEM and TEM images (IV). Reproduced from ref. 48 with permission from Journal of the American Chemical Society, Copyright 2017. (B) I. Two reversible redox states of a bipyridine-like structure. II. Sequential PSM processes of Py-BPY-COF to Py-Bpy^{2+}-COF or Py-$BPy^{+\bullet}$-COF. Reproduced from ref. 49 with permission from Journal of the American Chemical Society, Copyright 2019.

original COF (TpASH) were used to conjugate glycidol (Glc). Secondly, the surface hydroxy groups of Glc were used for conjugation of 3-aminopropyltriethoxysilane (APTES) to produce amine ($-NH_2$)-functionalized COFs. Thirdly, the free amino groups of the other end of the APTES molecules reacted with the carboxyl groups of FA through the EDC/NHS coupling reaction, resulting in the formation of the folate-conjugated targeted COF-based delivery system (TpASH-FA). This was the first case

of COF-based targeted drug delivery using sequential post-synthetic modifications.

Besides the active sites of the linkers, linkers with particular structures can also be target locations for PSM. Guo's team fabricated a 2,2′-bipyridine-based COF using sequential reactions *in situ*.[49] The obtained Py-BPy-COF contained a 2,2′-bipyridine-like structure whose dicationic derivatives could undergo two-step reversible reductions to form a radical cation and a neutral species (Fig. 6(B)-I), leading to the formation of two cationic types of COFs, Py-Bpy^{2+}-COF and Py-BPy$^{+\bullet}$-COF (Fig. 6(B)-II).

The bonding defect functionalization (BDF) was proposed by Dong's group in 2019, which is an alternative strategy to covalently connect the guest with the host.[50] In practical terms, the unbonded functional groups (bonding defects) at the end of the COF matrix are supposed to be ideal active sites for grafting small organic molecules (guest). For example, Dong's group prepared two boron-dipyrromethene (BODIPY)-decorated nanoscale COFs (NCOFs) through this BDF approach, *i.e.*, a Schiff-base condensation between the free end aldehyde groups (bonding defects in COFs) of NCOFs and the amino moieties of the organic photosensitizer BODIPY (Fig. 7(A)).[50] Similarly, through the BDF method, Dong's group also fabricated a COF-Fc nanosystem (Fig. 7(B)) through the Schiff-base condensation between the free end amino groups (bonding defects in COFs) of COFs and the aldehyde moieties of the Fenton-like reaction catalyst ferrocenecarboxaldehyde (FcCHO).[51]

2.3 Coordination bonding strategy for COF-based system

Monomers with specific structures sometimes are a powerful weapon for anchoring metal ions to obtain metalated COFs, which show great potential for biomedical application. For example, porphyrin-based COF nanoparticles were prepared and further coordinated with Fe^{2+} by Tang's group in 2021 (Fig. 8(A)).[52] Interestingly, the metalloporphyrin-based COF had high catalytic activity and enzyme-like property, which could effectively convert intracellular overexpressed H_2O_2 into highly toxic hydroxyl radical ($^{\bullet}$OH), *i.e.*, it exhibited chemodynamic therapy effects.

In 2020, Liu *et al.* fabricated a TAPB-DMTP-COF using two types of monomers, 1,3,5-tris(4-aminophenyl)benzene (TAPB) and 2,5-dimethoxyterephthaldehyde (DMTP).[53] Subsequently, to endow the platform with the ability to further catalyze and degrade the overexpressed H_2O_2 in the acidic tumor microenvironment (TME) through Fenton-like reactions, ferric chloride was introduced, by which Fe^{3+} could be coordinated with the amino groups of the COFs to form metallized COFs (Fig. 8(B)). The pre-synthesized CFAP nanocomposite showed efficacious synergistic photo-, chemodynamic-, and immunotherapy effects towards both the primary tumor and tumor metastasis.

In addition, COF-909-Cu with a bipyridine-like structure monomer is another typical example of metal coordination, which exhibited excellent CDT efficacy, and also efficiently triggered pyroptosis.[54] The adjacent tri-pyridines of 4,4′,4″-(1,4-phenylene)bis(([2,2′:6′,2″-terpyridine]-5,5″-dicarbaldehyde)) were ideal candidates for synthesizing metalated COFs. The tri-pyridine structure acted as a paw, which anchored the metal ions (*e.g.*, Cu^{2+}, Fe^{3+}, and Ni^{2+}) tightly, as illustrated in Fig. 8(C).

3. COFs for integration and delivery of small molecules, biomacromolecules and exosomes

Due to their large specific surface area and tunable pore size, COFs have been widely used as carriers for bioactives. Here, we classify COFs in three different groups according to the molecule size of the cargos they deliver, namely, small molecule@COF, biomacromolecule@COF and exosome@COF. The most studied small-guest molecules include anticancer drugs, such as DOX, 5-Fu, and cisplatin. Besides, COFs for the delivery of biomacromolecules has attracted interest from researchers

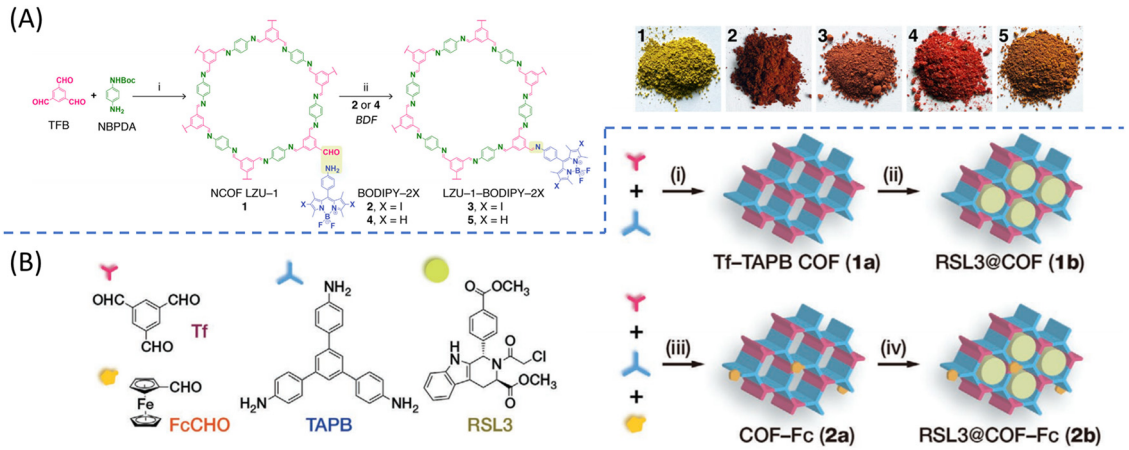

Fig. 7 Bonding defect functionalization (BDF). (A) Design of BODIPY-loaded nanoscale COFs and their photographs. Reproduced from ref. 50 with permission from iScience, Copyright 2019. (B) Material design and synthesis process of RSL3@COF-Fc. Reproduced from ref. 51 with permission from Small, Copyright 2021.

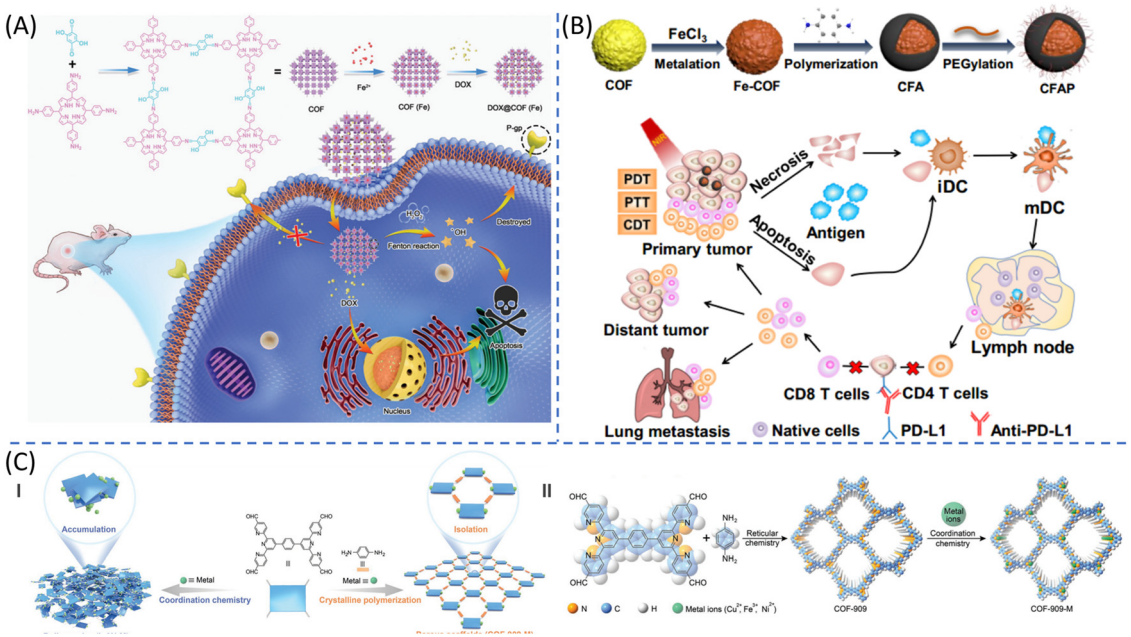

Fig. 8 Coordination bonding strategy. (A) Synthetic processes of DOX@COF(Fe) and its application. Reproduced from ref. 52 with permission from Chemical Communications, Copyright 2021. (B) Synthetic processes of CFAP and its application. Reproduced from ref. 53 with permission from ACS Applied Materials & Interfaces, Copyright 2022. (C) I. Illustration of the construction of bulk species (L-3N-M) or porous scaffolds (COF-909-M). II. Schematic diagram of multienzyme-mimicking COFs. Reproduced from ref. 54 with permission from Advanced Materials, Copyright 2022.

recently, especially for enzymes and genes. Surprisingly, COFs also work as an excellent choice for the delivery of more complicated targets, such as exosomes.

3.1 COFs for the integration and delivery of small molecules

Many anticancer drugs and other bioactive components with low molecular weight exhibit limited therapeutic outcomes due to their inherent properties such as low water solubility, poor bioavailability and short biological half-life. Furthermore, some traditional cytotoxic drugs can accumulate in tissues and organs, causing serious side effects. In this case, the construction of COF-based delivery platforms for small molecules is a powerful strategy to overcome the above-mentioned limitations. In fact, several researchers that have achieved success in this field.

In 2015, Fang and co-workers innovatively proposed that COFs have potential for drug delivery for the first time (Fig. 9(A)).[55] They fabricated two PI-based COFs, which were denoted PI-COF-4 and PI-COF-5, using a linear dianhydride and two different tetrahedral amines through an imidization reaction, exhibiting high crystallinity and considerable BET surface areas. The selected PI-COFs had pore sizes in the range of 11 Å to 15 Å, which provided sufficient room to entrap ibuprofen (IBU) molecules, which have a size of approximately 5 Å × 15 Å. Furthermore, the loading capacity of IBU was evaluated to be 24 wt% for PI-COF-4 and 20 wt% for PI-COF-5 based on the TGA analysis.

In the next year, compared with PI-COF-4 or PI-COF-5 on the micro-scale, nano-sized COFs were successfully fabricated, realizing tremendous progress for biomedical application. Bai *et al.* used 1,3,5-triformylbenzene and two types of amine compounds to synthesize two other polyimine-based COFs, namely, PI-3-COF and PI-2-COF (Fig. 9(B)).[56] Subsequently, by following one gold standard that the molecular size of the guest should fit well with the pore width of host, three different drug molecules (5-FU, captopril and IBU) were selected, resulting in a high DLC, which reached up to 30 wt%. Unlike the micro-scale PI-COF-4 and PI-COF-5 synthesized by Fang's group, the average diameter of PI-3-COF and PI-2-COF was about 50 nm, providing a greater possibility for applications *in vivo*. Moreover, the phenomenon that the drug-loaded COFs can be endocytosed in cancer cells was observed and confirmed by confocal laser scanning microscopy, providing direct evidence for nano COFs serving as drug carriers.

Subsequently, Guiyang Zhang *et al.* developed an amine-functionalized COF-1 (APTES-COF-1) to encapsulate DOX, which is a classic anticancer drug,[58] followed by decorating with fluorescent composite polyethylene-glycol-modified monofunctional curcumin derivatives (PEG-CCM), and then obtained a water-dispersible polymer-COF-DOX nanocomplex (Fig. 9(C)). Notably, this was the first time that COF-based nanocomposites were investigated for *in vivo* drug delivery and antitumor efficacy in nude mice, which can facilitate innovations and applications for COF-based carriers for drug delivery.

Recently, Yao and co-workers used this type of PSM strategy to functionalize TD-COFs with sodium phosphate groups in their channels to obtain phosphorylated COFs (SP-COFs), as shown in Fig. 9(D).[84] Interestingly, the hydroxyl unit ligands of TD-COFs were ideal phosphorylation sites, and it only took two simple steps to obtain the final product SP-COFs. After exploring

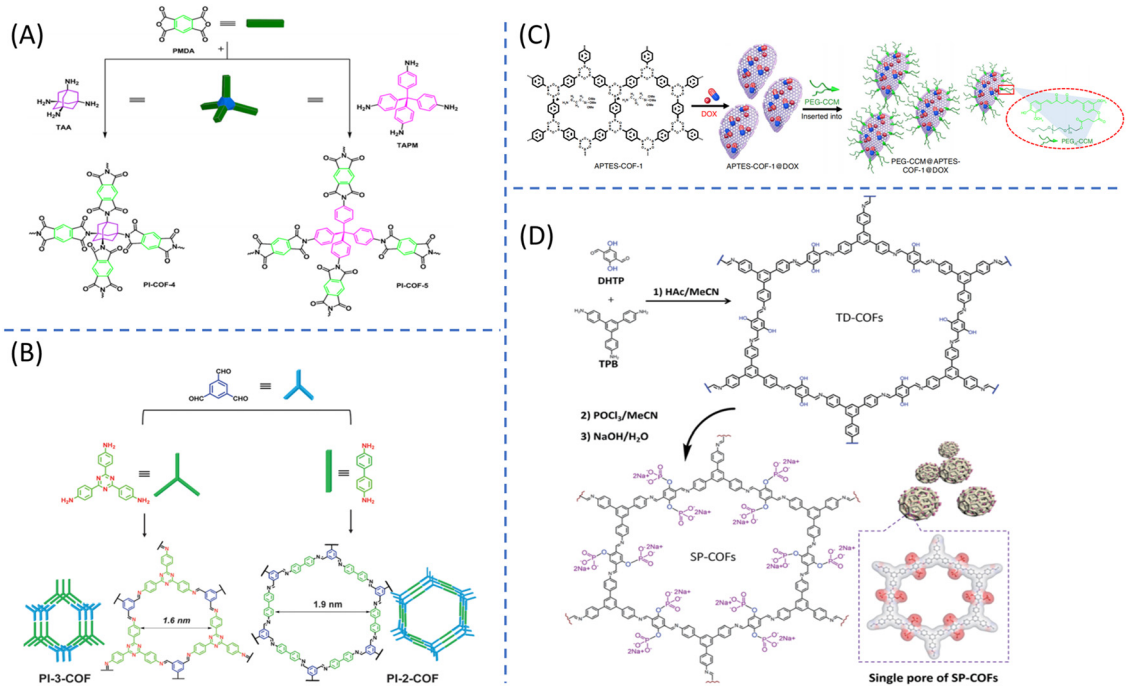

Fig. 9 Small molecule@COF. Synthesis process of (A) PI-COF-4 and PI-COF-5. Reproduced from ref. 55 with permission from the Journal of the American Chemical Society, Copyright 2015. (B) PI-3-COF and PI-2-COF. Reproduced from ref. 56 with permission from Chemical Communications, Copyright 2016. (C) DOX-loaded PEG-CCM@APTES-COF-1. Reproduced from ref. 58 with permission from Nature Communications, Copyright 2018. (D) Synthesis process of TD-COFs and SP-COFs. Reproduced from ref. 84 with permission from Chemical Science, Copyright 2022.

the mechanism of action between SP-COFs and the $A\beta_{42}$ peptide (a typical cytotoxin to Alzheimer's disease) through molecular dynamics simulation, the single pore of SP-COFs was proven to have potential for the recognition and targeting of specific amino acid sites of the $A\beta_{42}$ sequence. Besides, the following cellular level experiments also demonstrated that SP-COFs are new nano-inhibitors for the inhibition of Aβ fibrillation for the prevention and treatment of Alzheimer's disease.

In addition to drug molecules, COFs can also serve as carriers for photosensitizers (PSs) and photothermic agents (PTAs), where the former are employed photodynamic therapy (PDT), while the latter for photothermal therapy (PTT). Guan *et al.* prepared a nano COF-based system (VONc@COF-Por) through a facile synthetic approach under ambient conditions.[59] In this platform, porphyrinic PS (Por) was covalently grafted through the bonding defect functionalization strategy and the naphthalocyanine PTA (VONc) was noncovalently loaded *via* the guest encapsulation approach to obtain a multifunctional nanosystem for PDT/PTT combination therapy, as shown in Fig. 10(A). Quantitatively, the loading capacity of Por and VONc was determined by the UV-Vis external standard method and calculated to be 0.091 ± 0.010 and 0.256 ± 0.030 μmol mg^{-1}, respectively.

Various COF-based delivery systems for PSs and PTAs have successively emerged. Wang *et al.* developed the COF@IR783@CAD dual-delivery system for the combination of chemotherapy and PTT (Fig. 10(B)).[61] More importantly, this complex showed an excellent photo-absorption property and good light-to-heat conversion efficiency, suggesting that COF@IR783 can be used for photoacoustic (PA) imaging *in vivo*. Besides, Gan *et al.* constructed COF-1 using 1,4-benzendiborinic acid as a monomer for the delivery of ICG in 2019 (Fig. 10(C)).[109] Besides, Ge *et al.* obtained a TA-COF, which was synthesized using 1,3,5-triformyl-2,4,6-trihydroxybenzene (TP) and 4,4-azodiaminobenzene (AD) for the delivery of Ce6 in 2021.[68]

Recently, Zhang and co-workers designed a COF nanobowl and engineered it as an activatable nanosensitizer for the delivery of the small-molecule sonosensitizer Rose Bengal (RB) to realize activatable and ferroptosis-boosted sonodynamic therapy (SDT).[87] As shown in Fig. 10(D), COF nanobowls with high crystallinity and uniform morphologies were synthesized using a hard-template method. Benefiting from the MnO_x shell with glutathione (GSH)-responsive degradation behavior, the nanoplatform could switch from the "off" to "on" state to exert therapeutic efficacy at the tumor site under US irradiation.

3.2 COFs for the integration and delivery of biomacromolecules

COF-based carriers are not only good candidates for the delivery of small molecules, but also show a good performance for the immobilization of biomacromolecules. Nanomaterials with micropores are not ideal choices for the immobilization of biomacromolecules given that their pore sizes are too small to accommodate these large-sized biomolecules. By contrast, the pore size of COFs is designable, ranging from several to tens of angstroms, making mesoporous COFs popular materials for the encapsulation of biomacromolecules.

3.2.1 COFs for protein integration and delivery (protein@COF). Since the first reported work on the use of COFs as host

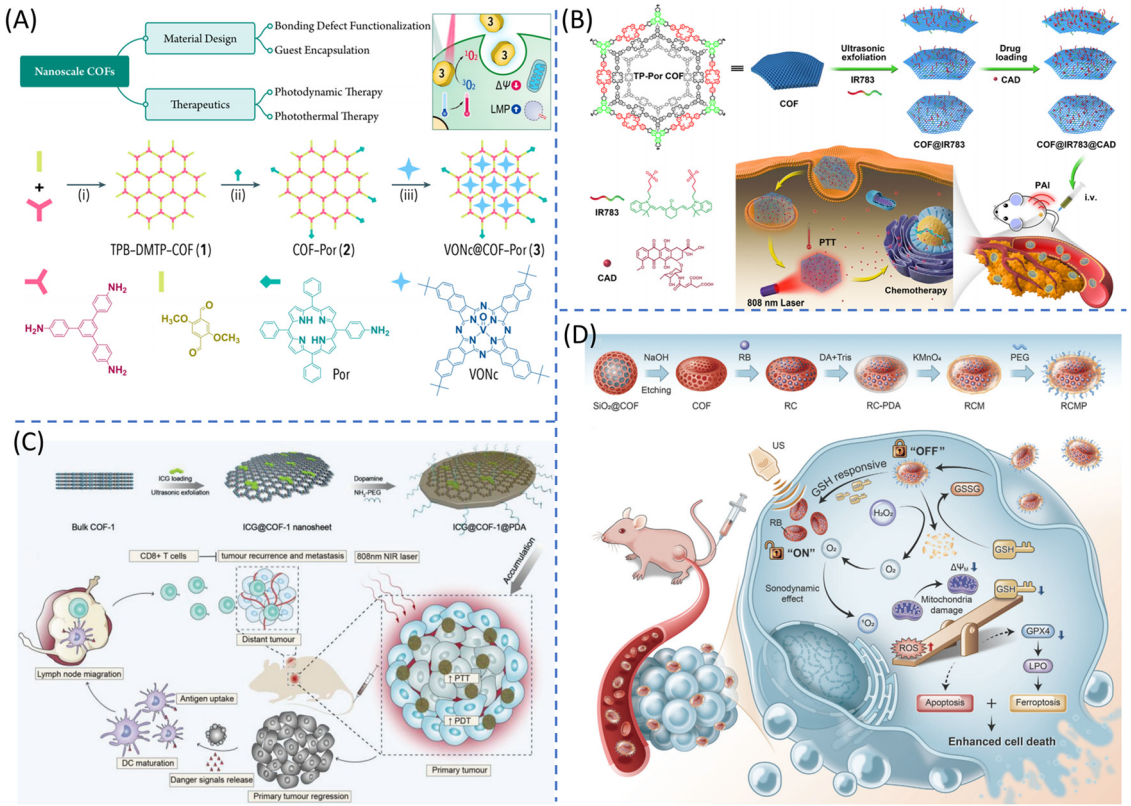

Fig. 10 Small molecule@COF. (A) Mind mapping for designing nanotherapeutic systems and synthesis process of VONc@COF-Por. Reproduced from ref. 59 with permission from ACS Nano, Copyright 2019. (B) Schematic illustration of synthesis of COF@IR783@CAD and its application. Reproduced from ref. 61 with permission from ACS Applied Materials & Interfaces, Copyright 2019. (C) Fabrication process and photoimmunotherapy performance of ICG@COF-1@PDA nanosheets. Reproduced from ref. 109 with permission from Advanced Functional Materials, Copyright 2019. (D). The synthetic process of RCMP and its application in SDT. Reproduced from ref. 87 with permission from Advanced Science, Copyright 2023.

materials for the immobilization of enzymes in 2015, many researches have proven that COFs as enzyme immobilization hosts can maintain the activity and stability of the immobilized enzyme.[88] For example, Wan *et al.* fabricated a COF-based nanopocket for the dual loading of GOx and CAT (Fig. 11(A)), which could generate cascade enzyme catalysis reactions and further give starvation therapy and enhanced photodynamic therapy.[96] After being labelled by Cy3 (a type of fluorescence dye), the loading capacity of GOx and CAT could be analyzed by a fluorescence spectrometer, with values of 46.1 μg mg^{-1} and 392.6 μg mg^{-1}, respectively. To further explore the retention time of free GOx and GOx@COF in tumor tissues, they were labelled with IR808 for fluorescence detection. The fluorescence intensity of COF@GOx-IR808 remained strong, even 5 days post-injection, indicating that GOx@COF could be retained for a long period to support complete catalysis.

In addition, ovalbumin (OVA) is a common antigen used for antigen-induced immunotherapy. Pang's group developed a COF-based antigen delivery system (named COF@ICG@OVA, CIO) for synergistic cancer phototherapy and immunotherapy (Fig. 11(B)).[93] The particle size of the composite material was measured to be ~100 nm, and the loading efficiency towards OVA was around 40.44%. More importantly, the CIO nanoparticle could not only ablate primary tumors through PDT/PTT, but also induce antitumor immune responses combined with checkpoint blockade therapy.

Recently, Xing *et al.* covalently immobilized cytochrome *c* (Cyt *c*) in $[OH]_{x\%}$-TD-COFs.[100] These COFs were synthesized using one triamine 1,3,5-tris(4-aminophenyl) benzene (TAPB) and two dialdehydes including 2,5-dihydroxyterephthalaldehyde (DHTA) and 2,5-dimethoxyterephthalaldehyde (DMTA) with different proportions (Fig. 11(C)), where *x*% represents the molar percentage of DHTA in the dialdehyde mixture. Therefore, the obtained COFs had different contents of anchoring sites (phenolic groups) for further introducing epoxy units on the channel walls of the COFs through a Williamson ether reaction. The third step was to anchor Cyt *c* in the COFs by the covalent linkage between nucleophilic groups from the enzyme guest (mainly the amino moiety) and epoxy groups from the COF host. Consequently, the covalent interactions between COFs and Cy *c* could induce secondary structural changes in the latter, resulting in a more accessible heme center, and thus enhancing the catalytic activity, which could reach 600% activity compared with the free enzyme.

Zhang *et al.* firstly prepared two borate-based COFs (COF-1 and COF-5) for the encapsulation of insulin (Ins) and glucose oxidase (GOx) *via* Brønsted and Lewis type (N: → B) complexation, and subsequently decorated them with polyethylene

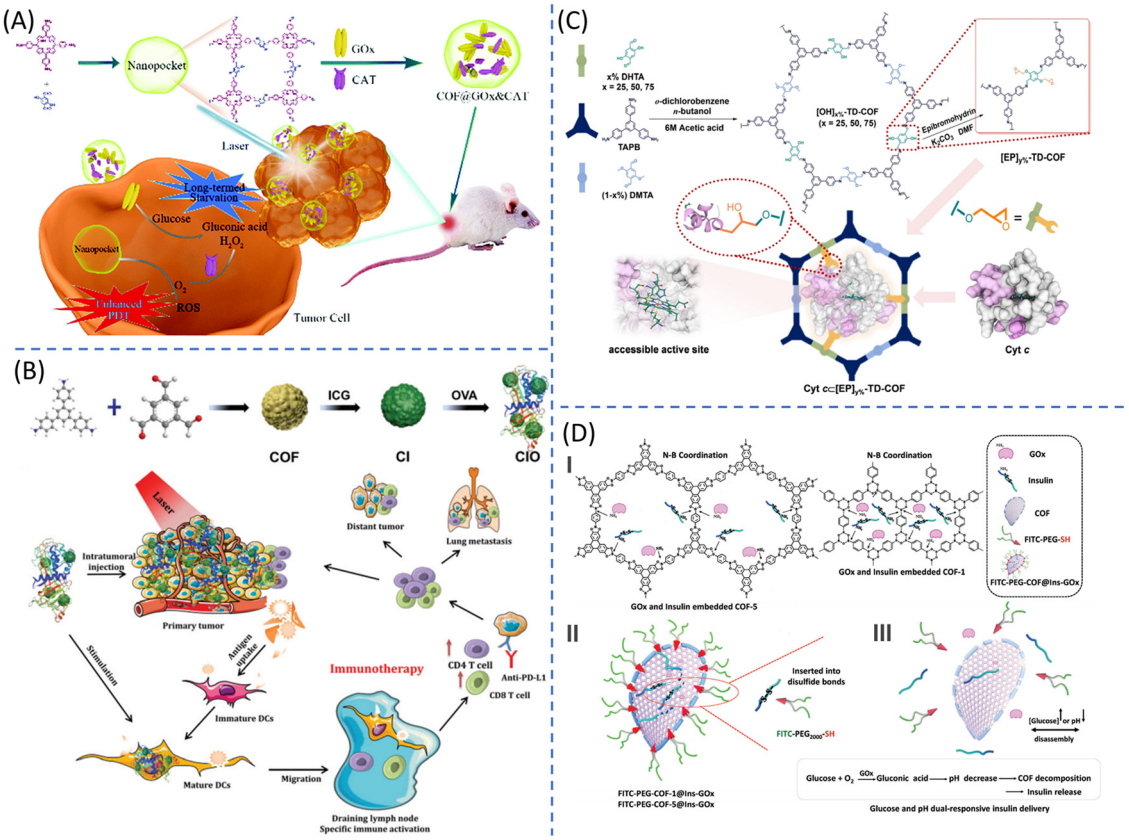

Fig. 11 Protein@COF. (A) Preparation of the COF@GOx@CAT nanopocket for cancer therapy. Reproduced from ref. 96 with permission from Chemical Communications, Copyright 2021. (B) The fabrication and mechanism of phototherapy and immunotherapy by CIO. Reproduced from ref. 93 with permission from Journal of Materials Chemistry B, Copyright 2020. (C) Covalent immobilization of Cyt c onto COFs. Reproduced from ref. 100 with permission from Angewandte Chemie-International Edition, Copyright 2022. (D) Synthesis of FITC-PEG-COF@Ins-GOx composites (I and II) and the possible mechanism of glucose and pH dual-responsive insulin delivery (III). Reproduced from ref. 94 with permission from ACS Applied Materials & Interfaces, Copyright 2019.

glycolated isothiocyanate (FITC-PEG) to finally obtain FITC-PEG-COF@Ins-GOx (Fig. 11(D)).[94] The obtained composite was suggested to achieve the glucose- and pH dual-responsive delivery of COF-based insulin. Due to the presence of fluorescein FITC, the bio-distribution of the composite could be seen by tracking the intrinsic fluorescence of FITC *in vivo*. Besides, this composite showed excellent anti-diabetic effects on type I diabetic mice and could maintain the blood glucose level in the normal range.

In addition to intravenous delivery, COFs could also be used for the oral delivery of insulin. Farah Benyettou and co-workers prepared layered 2D COF nanosheets with insulin loaded between the nanosheet layers (TTA-DFP-nCOF/insulin) with a high loading capacity (~65 wt%).[95] It was noteworthy that TTA-DFP-nCOF could protect the encapsulated insulin to maintain its activity under harsh conditions mimicking the stomach environment (pH = 2.0); meanwhile, the sustainable release of insulin could be successfully implemented under hyperglycemic conditions.

3.2.2 COFs for nucleic acid integration and delivery (nucleic acid@COF). In addition to proteins, COFs can also serve as carriers for other biomacromolecules, *i.e.*, genes. For instance, Tang's group prepared a COF-based platform for integrating a dye-labeled oligonucleotide in the carriers.[92] Compared with the monomer porphin, the porphin-based COF had a better crystalline reticular structure and large planar structure with strong π-electron system, making the latter easy to absorb DNA single strands (Fig. 12(A)). The relative fluorescence intensity of the COF–survivin system changed slightly during incubation in PBS or DMEM for 7 days, indicating that it had a good stability. Also, the system possessed the ability to selectively image cancer through fluorescence resonance energy transfer (FRET) with a 'turn-on' pattern. Besides, the porphin-based COF could generate abundant $^1O_2$ species under NIR laser irradiation, inducing cancer cell apoptosis without dark toxicity.

Cao *et al.* reported a strategy to construct triazine-based COF nanosheets (CTF-PEG-PEI) *via* exfoliation and surface modification for the delivery of DNA (Fig. 12(B)).[99] This nonviral vector had a unique brush-like hierarchical structure, making it strongly condense nucleic acids and efficiently release the nucleic acid cargo after cellular uptake. To further study the *in vivo* gene delivery ability of COFs, Hao *et al.* designed a series of cationic porous COF-based nanoparticles with a good gene transfection effect and biocompatibility (Fig. 12(C)).[110] After successfully constructing the vehicles, a therapeutic gene

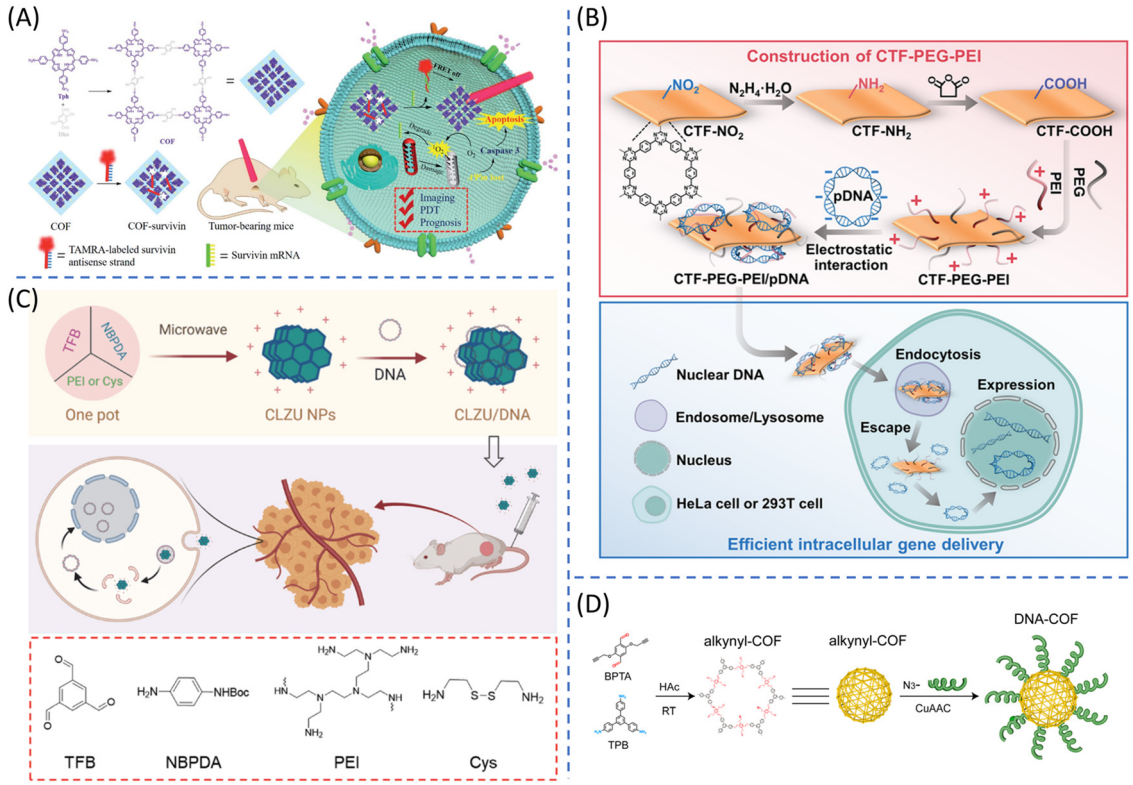

Fig. 12 Nucleic acid@COF. (A) Synthesis of the COF–survivin system. Reproduced from ref. 92 with permission from Chemical Science, Copyright 2020. (B) Construction of CTF-PEG-PEI for efficient intracellular gene delivery. Reproduced from ref. 99 with permission from ACS Applied Nano Materials, Copyright 2021. (C) Construction of CLZU nanoparticles and their application for anti-tumor gene therapy. Reproduced from ref. 110 with permission from Science Chins Chemistry, Copyright 2021. (D) Construction of DNA-COFs for the detection of exosomes. Reproduced from ref. 103 with permission from Analytical Chemistry, Copyright 2022.

for tumor suppression, shVEGF, was chosen for *in vivo* delivery. Finally, this platform could significantly inhibit tumor growth, indicating its excellent potential for gene therapy.

Yang's group firstly proposed a strategy to functionalize COFs with DNA by covalent interaction.[103] As shown in Fig. 12(D), the azide-modified DNA could be efficiently connected to the pre-prepared alkynyl-rich COFs through Cu(I)-catalyzed azide/alkyne cycloaddition (CuAAC) reaction. Then, a complementary 5-carboxyfluorescein-labeled DNA (FAM-DNA) strand was used to hybridize with the single-strand DNA on the COF surface to obtain DNA@COF composites. In this design, the COF probes were further used to construct an effective electrochemical biosensor for the detection of exosomes.

3.3 COFs for the integration and delivery of exosomes (exosome@COF)

More impressively, COFs have potential to deliver more complex objectives, such as exosomes. Sun *et al.* designed and fabricated a 2D COF-based nanoagent for the delivery of antibacterial immuno-engineered exosomes, which was designated as PCOF@E-Exo.[108] This COF, TPB-DHTA-COF, was synthesized through the polycondensation of 1,3,5-tris-(4-aminophenyl) benzene (TPB) and 2,5-dihydroxyterephthalaldehyde (DHTA), with a 3.3 nm pore diameter and a 3.2 Å neighboring layer size, as shown in Fig. 13. Furthermore, the surface functionalization of COFs was accomplished by introducing polydopamine to overcome their poor water dispersibility and inefficient intracellular uptake efficiency. Subsequently, the engineered exosomes were integrated in a PCOF nanosheet platform *via* simple electrostatic interaction. The TEM image (Fig. 13(II)) of PCOF@E-Exo proved the abundant binding of E-Exos to the PCOF nanosheets, which were marked with blue arrows. Additionally, the prepared PCOF@E-Exos remained stable and relatively uniform in various solvents, such as deionized water, PBS, fetal bovine serum (FBS, 10%) and DMEM medium. As shown in Fig. 13(IV), the PCOF@E-Exo-integrated nanoagent showed excellent antibacterial activity towards both Gram-negative (*Escherichia coli*) and Gram-positive (*Staphylococcus aureus*) bacteria.

4. COF-based hybrid materials for the integration and delivery of bioactives

Hybrid materials are expected to make up for the original deficiencies of their components or enhance their advantages to realize 'the whole is greater than the sum of the parts'. Impressively, COFs show good potential as hybrid material candidates,[111] and researchers have begun to combine COFs with other functional materials to prepare COF-based composites for

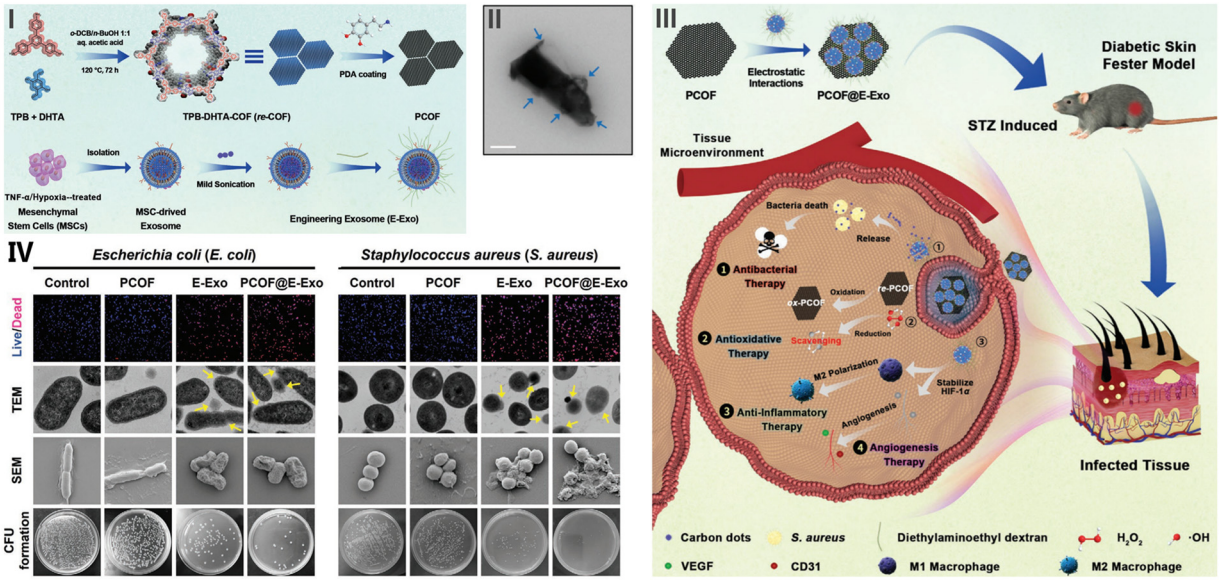

Fig. 13 Exosome@COF. I. Formation of TPB-DHTA-COF, synthesis of PCOF, and preparation of engineered exosome (E-Exo). II. TEM image of the PCOF@E-Exo nanoagent. III. Preparation of the PCOF@E-Exo integrated nanoagent and its theranostic mechanism in infected diabetic fester wounds. IV. Antibacterial activity analysis of the PCOF@E-Exo nanoagent against *E. coli* and *S. aureus*. Reproduced from ref. 108 with permission from Small, Copyright 2022.

Table 2 Summary of COF-based hybrid composites for cargo integration and delivery

Year	Composite	Hybrid type	Cargo	Applications	Ref.
2019	ICG@COF-1@PDA	PDA@COF	ICG	Immunotherapy/PTT	109
2020	HRP-pSC4-AuNPs@COFs	Au NP@COF	HRP	Exosomes detection	112
2023	ICPA	Pt NP@COF	ICG	Self-strengthening photocatalytic therapy	113
2019	Co-MOF@TPN-COF	MOF@COF	Aptamer	Ampicillin detection	114
2021	Cu-MOF@CuPc-TA-COF	MOF@COF	pDNA	HIV-1 DNA detection	115
2021	Cu-MOF@TpBD-COF	MOF@COF	Aptamer	PDGF-BB detection	116
2022	MOF@COF-Apatinib	MOF@COF	Apatinib	MWDT/anti-angiogenesis therapy	117
2022	CA4V/ZIF-90@TzCOF@Apt	MOF@COF	CA4V	Anti-vascular therapy	118
2022	C_{60}@TAPT-DHTA-COF	C_{60}@COF	Aptamer	Tobramycin detection	119
2022	O_2-FeCOF@$CaCO_3$@FA	$CaCO_3$@COF	FA	PDT/Ca^{2+} overload treatment	120
2021	Au/COF/MnO_2	MnO_2@COF@Au NP	Antibody	HCG detection	121
2021	Fe_3O_4@COF-BSA–FA	Fe_3O_4@COF	DOX	PTT/CT	122
2021	Fe_3O_4@COF@BSA	Fe_3O_4@COF	BSA	Chiral recognition	123
2022	Fe_3O_4@SiO2@COF	Fe_3O_4@SiO_2@COF	Hairpin DNA	Glioma detection	124
2022	Fe_3O_4@COF-Au NP	Fe_3O_4@COF@Au NP	ssDNA	ATP detection	125
2023	GOx–Fe_3O_4@COF	Fe_3O_4@COF	GOx	Removal of mycotoxins	126
2023	MnO_2-Poly(I:C)@COF	MnO_2@COF	Poly(I:C)	Immuno-sonodynamic therapy	127
2022	$M_GP_PC_LP$	SiO_2@COF	Gemcitabine/glycoprotein Inhibitor/losartan	Programmed multi-drugs delivery	128
2022	OC-COF	Cyclodextrin@COF	Ligustrazine (LIG)	Inhalation therapy against acute lung injury	129
2023	Por-COF-gel	Gel@COF	Acrylate	Sterilization/wound healing	130
2023	CuS@COFs-BSA–FA/DOX	CuS@COF	DOX/BSA	CT/PTT/CDT	131

the delivery of cargo, such as MOF@COFs, metal NP@COFs, metal oxide/sulfide@COFs, silica@COFs, and polymer@COFs. Table 2 summarizes the COF-based hybrid composites reported for the delivery of cargo in the last three years.

4.1 MOF@COFs

It is a good strategy to combine MOFs and COFs to realize a collaborative functional effect. One the one hand, the limitation of COFs of the lack of active metal centers can be addressed by introducing metal complexes in COFs. On the other hand, the restriction that the relatively weak strength of coordination bonds of MOFs can be strengthened by encapsulating other functional materials.

For example, Li *et al.* proposed the combination of a COF-based nanocapsule with an MOF (MOF@COF) for loading the hydrophobic inhibitor apatinib.[117] The MOF as the inner layer consisted of Bi^{3+} and Mn^{2+}, which was designed as a microwave sensitizer to generate cytotoxic $^1O_2$ and heat for microwave

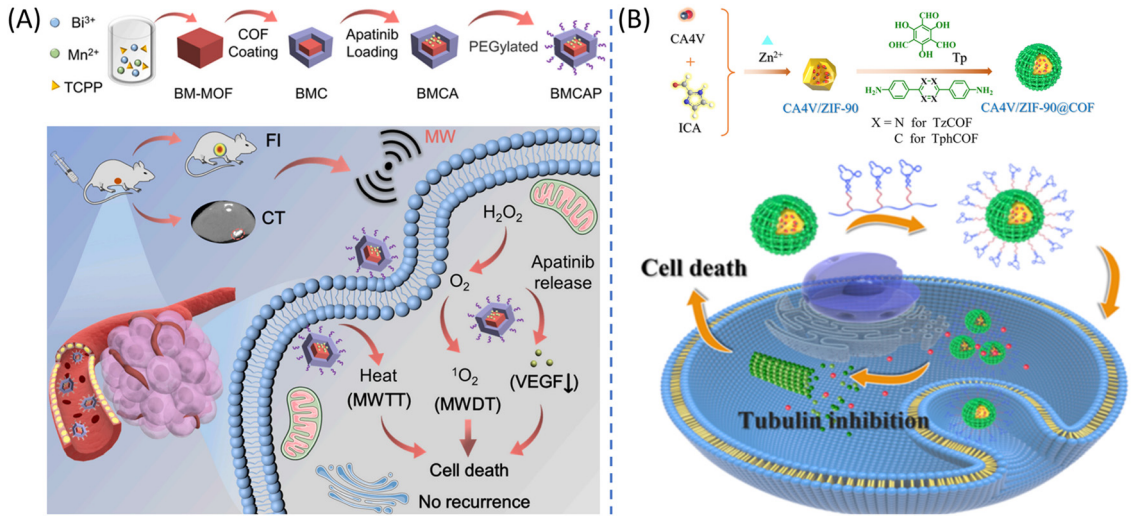

Fig. 14 MOFs@COFs. (A) Synthesis of BMCAP nanocapsule and its application in MWDT/MWTT for anti-angiogenesis of colorectal cancer. Reproduced from ref. 117 with permission from Biomaterials, Copyright 2022. (B) Synthesis of CA4V/ZIF-90@COF@Apt nanoreactor and its significant cancer inhibition rates towards DU145 cells. Reproduced from ref. 118 with permission from Chemical Communications, Copyright 2022.

dynamic/thermos synergistic therapy (MWDT/MWTT), as shown in Fig. 14(A). The COF as the outer layer was covalently coated on MOF for further augmenting these two treatment effects. Besides, Wang *et al.* proposed a bioorthogonal nanoreactor (CA4V/ZIF-90@TzCOF@Apt) with a ZIF-90 core and COF shell (Fig. 14(B)).[118] Specifically, the ZIF-90 core was used for the delivery of CA4V, a prodrug of the vascular disrupting agent CA4, through a 'one-pot' *in situ* self-assembly process, involving CA4V, imidazole-2-carboxaldehyde (ICA) and Zn^{2+}. Besides, the TzCOF shell was utilized for coating an aptamer polymer, which could target tumor cells.

4.2 Metal nanoparticle@COFs

COFs can be functionalized with metal nanoparticles such as Au NPs, and Pt NPs, and the resulting composites have extensive application prospect. For instance, Wang *et al.* designed a novel COF-based nanoprobe (HRP-pSC4-AuNPs@COFs), whose surface was decorated with AuNPs, which were further used for the immobilization of horseradish peroxidase (HRP) (Fig. 15(A)).[112] Notably, the COF could not only load a large amount of HRP due to its high porosity, but also maintain the functionality of HRP owing to its exoskeleton support. The AuNPs were used for accelerating the migration of charge carriers and improving the response of biosensors. Consequently, the whole design showed an excellent analytical performance for the detection of colorectal cancer-derived exosomes, even in clinical serum samples.

Recently, increasing efforts have been devoted to the combination of functional components, *i.e.*, metal nanoparticle-doped COFs. Tang's group proposed the preparation of ultra-small Pt NPs deposited on a COF nanoplatform (termed CP) *via* an *in situ* chemical reduction method (Fig. 15(B)).[113] Subsequently, a thiol-terminated AS1411 aptamer was decorated on it by forming a stable Pt–S bond and the photosensitizer ICG was loaded to obtain the final versatile nanosystem (ICPA).

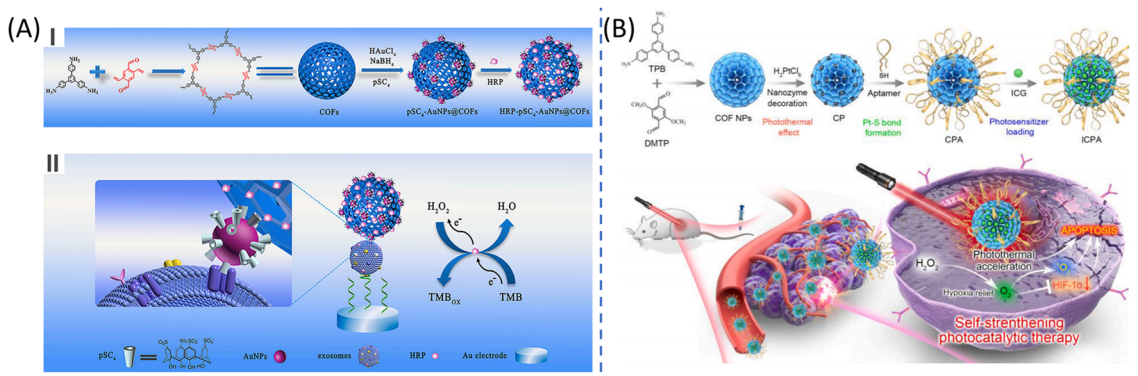

Fig. 15 Metal nanoparticles@COFs. (A) I. Process for the fabrication of COF-based nanoprobes and II. mechanism of the electrochemical biosensor for the detection of exosomes. Reproduced from ref. 112 with permission from Biosensors and Bioelectronics, Copyright 2020. (B) Synthesis process of ICPA and its application in reversing tumor hypoxia and inducing tumor thermal damage and oxidative stress. Reproduced from ref. 113 with permission from Biomaterials, Copyright 2023.

4.3 Metal oxide/sulfide@COFs

Metal oxides or sulfides play an important role in biomedical applications because of their metal active sites and intrinsic enzyme-mimicking abilities. Recently, Liu's group fabricated well-defined COFs with sonosensitive properties for the efficient loading of the toll-like receptor agonist, Poly(I:C), as well as *in situ* growth of MnO_2, which acts as an enzyme-like nanocatalyst for oxygen production by reacting with TME-overexpressed H_2O_2.[127] Finally, the prepared MnO_2-Poly(I:C)@COF composites were successfully used for imaging-guided cancer combinatorial immuno-sonodynamic therapy, as illustrated in Fig. 16(A).

Zhao *et al.* integrated a magnetic COF with Fe_3O_4 shell and further functionalized it with bovine serum albumin (BSA) and folic acid (FA) to improve its dispersibility and selectivity.[122] Finally, the prepared novel Fe_3O_4@COF-BSA–FA nanosystem worked as an effective DOX carrier with excellent photothermal performance, resulting in chemo/photothermal combined therapy (Fig. 16(B)). Similarly, Wang *et al.* established a multifunctional nanoplatform (CuS@COFs-BSA–FA/DOX) based on a hybrid CuS/COF inner layer and BSA/FA outer layer for synergistic chemo/photothermal/chemodynamic therapy (Fig. 16(C)).[131]

5. Stimuli-responsive release in COF-based system

The key to drug delivery systems is not only about their high loading capacity, but also their ability to act as vehicles that can release cargos in a stimuli-responsive, controllable and sustained manner over time. In this part, we introduce a variety of stimuli-responsive COFs that can achieve the regulated delivery and controlled release of loaded cargos upon activation by diverse stimuli, such as pH, GSH, hypoxia, and albumin. Table 3 summarizes the recent studies on COF-based stimuli-responsive release systems.

5.1 pH-responsive COFs

Among the COF-based carriers triggered by internal stimuli, pH-responsive COFs are the most widely studied biomaterials, especially for cancer therapy, because of the acidic TME and the sensitivity of imine bonds to external pH values. Specifically, the large amount of H^+ tends to induce the protonation of the nitrogen atoms of –C═N– bonds under low pH conditions, which decreases the hydrophobic interaction between the cargo and COF, achieving a pH-responsive and controlled release profile. For example, Lalehan Akyuz designed and fabricated an imine-based COF (DT-COF) for the further delivery of an antineoplastic drug, carboplatin, with a significant loading capacity of 31.32%.[62] More importantly, to determine the *in vitro* drug release kinetics, three models (zero order, first order, and Higuchi models) were used to explain the drug release mechanism of carboplatin from the CP-DT-COF nanospheres, and the final results suggested that the Higuchi model based on Fickian diffusion was the most suitable model for drug release. Besides, the drug release performance was recorded at pH = 7.4 (physiological pH of normal cells) and pH = 5.0 (physiological pH of cancer cells). Under both conditions, the release profile for CP-DT-COF was observed to be fast release in the first 12 h, followed by continuous and sustained release over 120 h. However, the drug releasing rate at pH = 5.0 was higher than that at pH = 7.4, suggesting that CP-DT-COF

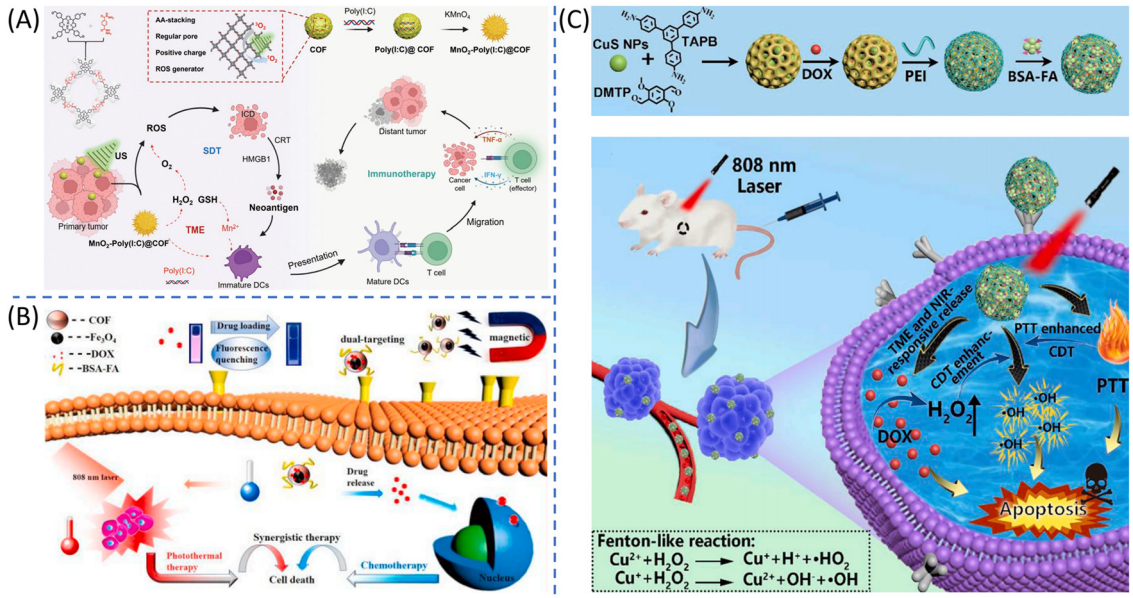

Fig. 16 Metal oxides/sulfides@COFs. (A) Construction of MnO_2-Poly(I:C)@COF NPs for enhanced SDT. Reproduced from ref. 127 with permission from Advanced Functional Materials, Copyright 2022. (B) Synthesis of Fe_3O_4@COF-BSA–FA system and its synergistic treatment. Reproduced from ref. 122 with permission from Microporous and Mesoporous Materials, Copyright 2021. (C) Preparation and therapeutic functions of CuS@COFs-BSA–FA/DOX. Reproduced from ref. 131 with permission from Chemical Engineering Journal, Copyright 2023.

Table 3 Summary of recent studies on COF-based stimuli-responsive release systems

COF	Linkage	Stimuli type	Morphology and size	Cargo	Release behavior	Disease model	Ref.
TAPB-DMTP-COF	Imine	pH	Nanosphere (200–400 nm)	DOX	Almost 100% at pH = 5.0 in 24 h	H22 xenograft mouse model	42
TAPB-DMTA-COF	Imine	pH	Multiantenna-like particle (160.5 nm)	Curcumin	74.6% at pH = 5.0 in 100 h	Animal full-thickness wound defect model	43
DT-COF	Imine	pH	Nanosphere (500–600 nm)	Carboplatin	Completely released for 1 h at pH = 5.0 and 12 h at pH = 7.4	—	62
Tf-TAPB COF	Imine	pH	Nanosphere (~170 nm)	RSL3	61.1% ± 9.0% at pH = 5.0 in 96 h	HT-1080 xenograft mouse model	51
TPB-DMTP-COF	Imine	pH	Radial sphere (144 nm)	Gambogic acid	59.43% at pH = 5.0 in 24 h	4T1 xenograft breast cancer model	132
COF-366	Imine	pH	Sphere (~150 nm)	Plumbagin	93% at pH = 5.5 in 72 h	LNCap cells	74
Hollow COF	Imine	pH	Hollow nanosphere (~30 nm shell thickness)	Apatinib	76.3% at pH = 5.7 in 24 h	HepG2 xenograft mice	83
TTA-DFP-nCOF	Imine	pH	Nanosheet (stacking of ~18 layers)	Insulin	Almost 100% at pH = 7.4 with 5 mg mL^{-1} glucose after 7.5 h	Streptozotocin-induced type 1 diabetic rat model	95
PI-CTF	Triazine	pH	Tubular structure (~30 nm)	Sorafenib	66% at pH = 5.3 in 48 h	LNCaP cells	60
JUC-56-$[HZ]_x$	Hydrazone	pH	—	Cytarabine	74.56% at pH = 4.8 in 72 h	—	71
F68@SS-COF	Imine and disulfide	pH/GSH	Nanosphere (140 ± 15 nm)	DOX	90% at pH = 5.0 with 10 mM GSH in 24 h	HepG2 cells	64
HY/SS-CONs	Imine and disulfide	pH/GSH	Nearly sphere (120 ± 20 nm)	DOX	About 90% at pH = 5.0 with 10 mM GSH in 72 h	HepG2 cells	66
DSPP-COF	Imine and disulfide	pH/GSH	59 nm	5-Fu	~96.9% at 10 mM GSH in 24 h	MCF-7 xenograft nude mouse	86
TPE-ss COF	Imine and disulfide	pH/GSH	Nanosheet (5 nm thickness)	Matrine	~80% at pH = 5.0 with 10 mM GSH in 80 h	Myocardial ischemia/ reperfusion injury	76
Dise-Por	Imine and diselenide	pH/GSH/photo	Sheet-like morphology	DOX	89.6% at pH = 5.4 with 10 mM GSH and 808 nm laser in 96 h	PC-3 tumor xenografted mice	80
TA-COF	Imine and azo	Hypoxia	Sphere-like (90 nm)	TPZ	~65% with 2 mM $Na_2S_2O_4$ in 2 h	4T1 tumor xenografted model	68
PER@PDA-COF-1	Imine	Protein	Nanosheet	Mitoxantrone	UV-Vis absorption increase and shift when adding 0.3 mM human serum albumin	CT-26 tumor xenografted model	79
THPPTK-PEG	Thioketal	Photo/hypoxia	Nanoparticle	AQ4N	78.79% after 4 h with a 660 nm laser	4T1 xenograft breast cancer model	40
Nano TKPP-COF	Dithioketal	Photo	Nanoparticle	DC_AC50	97.7% in 12 h with a 660 nm laser	HT-1080 xenograft mouse model	133

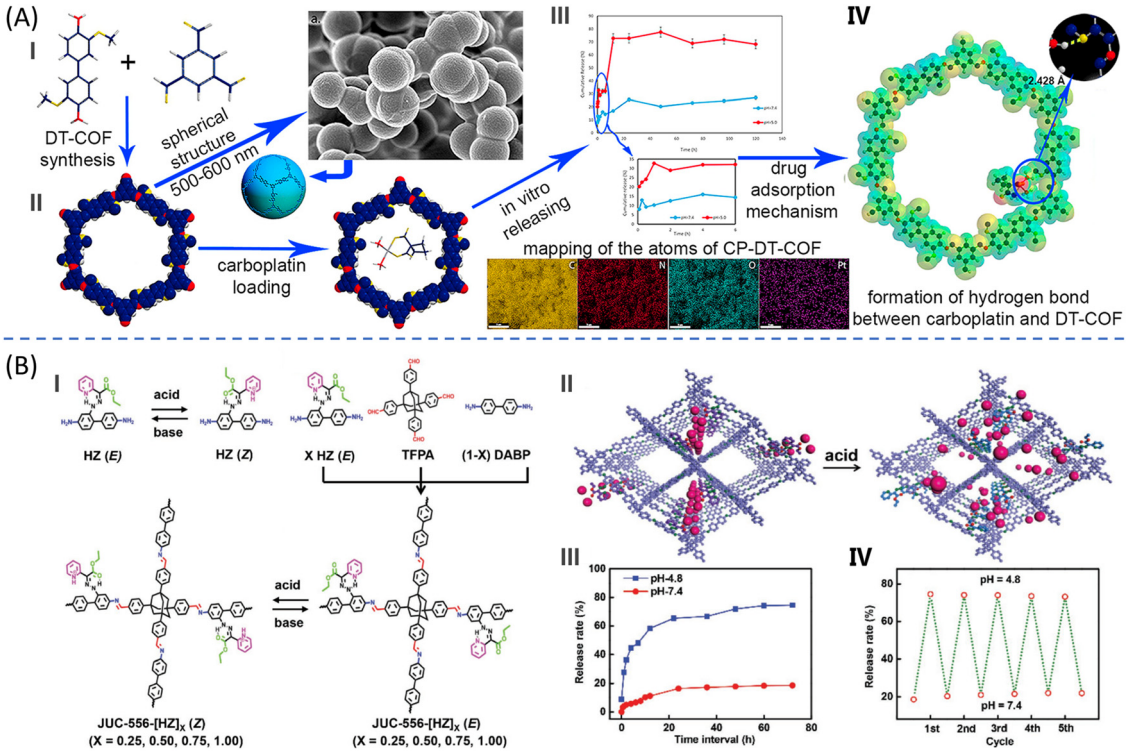

Fig. 17 pH-responsive COFs. (A) I. Schematic diagram of chemical structure of DT-COF. II. Schematic representation of the loading of carboplatin. III. Drug release profiles of carboplatin-loaded DT-COF. IV. Formation of a hydrogen bond between carboplatin and DT-COF from DFT calculation. Reproduced from ref. 62 with permission from Microporous and Mesoporous Materials, Copyright 2020. (B) I. Schematic representation for preparing JUC-556-$[HZ]_X$ with *E*/*Z* isomerization. II. Release of Ara-C from the channels of JUC-556-$[HZ]_X$ in acidic solution. III. Drug release profiles and IV. reversibility of Ara-C-loaded JUC-556-$[HZ]_{0.50}$ in a simulated cancer fluid. Reproduced from ref. 71 with permission from Small, Copyright 2021.

exhibited pH-dependent release, as illustrated in Fig. 17(A). Moreover, a DFT theoretical calculation was used to investigate the interaction forces between carboplatin and the DT-COF carrier. Geometry optimization and interaction energy calculations demonstrated that the guest molecule preferentially interacted with the imine nitrogen and methoxy oxygen of the host CP-DT-COF.

Fang's group constructed two 3D pH-triggered COFs based on a hydrazone derivative with E/*Z* interconversion, with the abbreviations of JUC-556-$[HZ]_x$ (*Z*) and JUC-556-$[HZ]_x$ (*E*), where x was the proportion of one of the linkers HZ (x = 0.25, 0.50, 0.75, or 1.00).[71] These functionalized COFs were used for loading cytarabine (Ara-C) in a pH-responsive way. Specifically, the addition of acid (trifluoroacetic acid, TFA) or base (triethylamine, Et_3N) induced *E*/*Z* isomerization in the dissociative HZ units, which could be inspected by UV-vis absorption spectroscopy, showing a characteristic absorption band at 249 nm for *Z* isomerization and 263 nm for *E* isomerization. Finally, JUC-556-$[HZ]_{0.50}$ displayed the best performance in terms of drug release, which reached 74.56% in pH = 4.8 buffer within 72 h, while only 18.59% in pH = 7.4 buffer, as illustrated in Fig. 17(B).

5.2 Redox-responsive COFs

Cellular redox homeostasis provides a vital function for life and the normal physical activity of cells. Thus, tipping the redox balance may be beneficial to get rid of harmful cells. Based on this idea, COFs with particular building blocks have been designed and fabricated, which are sensitive to the overexpressed GSH in the TME. The protonation and oxidation of disulfide or diselenium groups in COFs tend to initiate drug release upon exposure to GSH. Zhang's group firstly proposed a GSH-responsive COF (denoted as F68@SS-COF) using commercially available disulfide-bearing building blocks to efficiently encapsulate and deliver DOX.[64] Due to the presence of rich disulfide bonds in COFs, F68@SS-COFs were expected to disintegrate in the presence of GSH, which was overexpressed in the tumor intracellular microenvironment. This was demonstrated by the experimental results, where the DOX release from F68@SS-COFs in the presence of GSH (over 90% in 24 h) was significantly higher than that in the absence of GSH (about 40% release in 24 h), as shown in Fig. 18(A).

Recently, Dong's group constructed a host–guest supramolecular system (5-Fu⊂nano DSPP-COF) by immersing nano DSPP-COF in a 5-Fu methanol solution at room temperature for 24 h, and the loading content of 5-Fu was calculated to be around 0.86 μmol mg^{-1}.[86] The disulfide-involved DSPP-COF showed GSH-triggered biodegradability as expected, which was verified by the experimental results, where up to ~96.9% of the encapsulated 5-Fu was released from 5-Fu⊂nano DSPP-COF with the external environment of a 10 mM GSH buffered solution, while only ~11.3% 5-Fu was observed without GSH (Fig. 18(B)). In addition to TME that overexpresses GSH, the

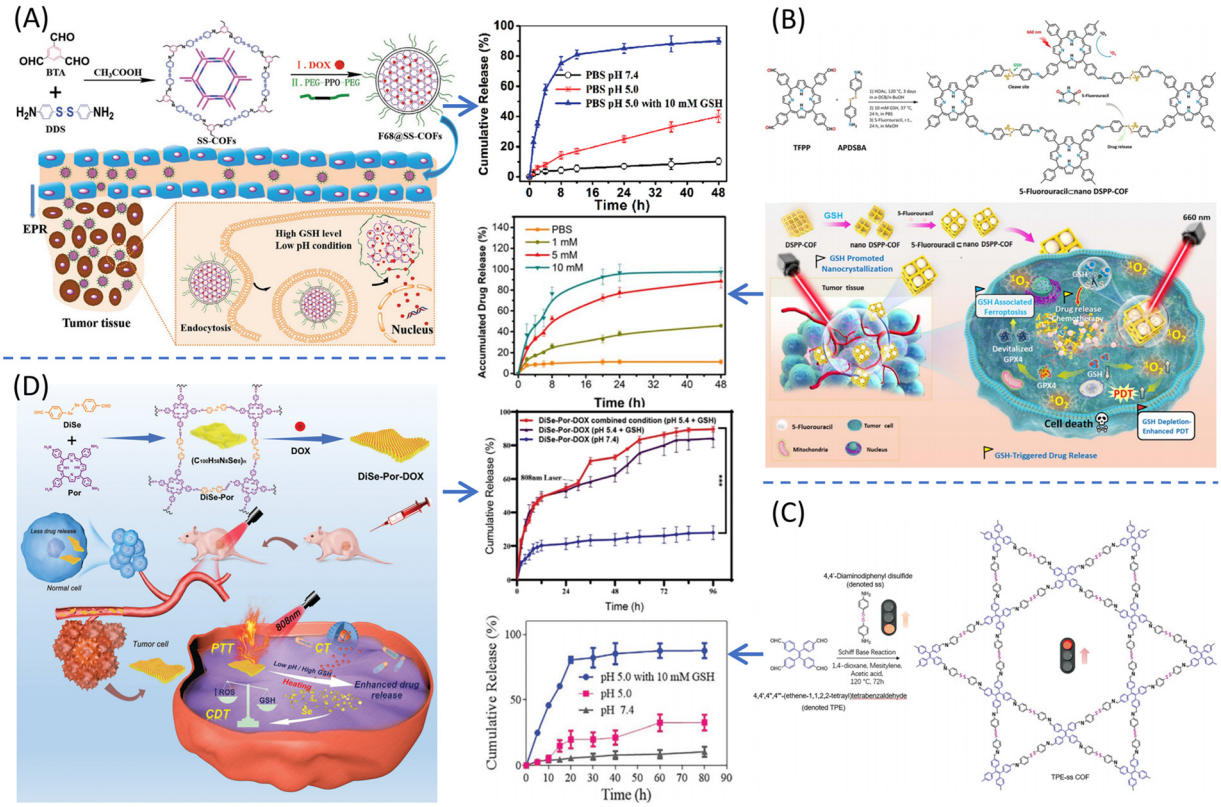

Fig. 18 Redox-responsive COFs. (A) Preparation of drug-loaded F68@SS-COFs and their intracellular GSH-responsive drug release. Reproduced from ref. 64 with permission from Macromolecular Rapid Communications, Copyright 2020. (B) Synthesis of 5-Fu⊂nano DSPP-COF and its treatment application, and the 5-Fu release behavior triggered by GSH with different concentrations. Reproduced from ref. 86 with permission from Chemical Science, Copyright 2023. (C) Preparation of matrine-loaded TPE-ss COF (TPE-ss COF@matrine) and intracellular GSH-responsive drug release. Reproduced from ref. 76 with permission from Small, Copyright 2022. (D) Schematic illustration of DiSe-Por-DOX for combination antitumor therapy and drug release curves with different conditions. Reproduced from ref. 80 with permission from Journal of Materials Chemistry B, Copyright 2022.

intracellular myocyte microenvironment also undergoes overexpression of GSH after ischemia-reperfusion injury. Thus, Huang *et al.* designed a redox-responsive COF (TPE-ss COF) as an effective drug delivery carrier for matrine, an anti-cryptosporidial drug.[76] As shown in Fig. 18(C), the matrine-loaded TPE-ss COF composite (TPE-ss COF@matrine) exhibited an evident GSH-dependent release profile, where over 90% of loaded drugs was released from the COF within 80 h in response to the condition of pH = 5.0 and 10 mM GSH, while only about 30% or 10% release could be seen under pH = 5.0 or 7.4 in the same period.

Interestingly, Lou *et al.* prepared a diselenium-bridged COF (DiSe-Por-DOX) for the effective encapsulation and highly controlled release of DOX.[80] When internalization in tumor cells, the disrupting of diselenium bonds (Se–Se) in the high GSH tumor internal environment could not only promote the release of DOX, but also boost the generation of intracellular ROS, which broke the redox homeostasis of cancer cells (Fig. 18(D)). As expected, the release of DOX increased with a decrease in acidity (pH = 7.4/6.5/5.5) or increase in the GSH concentration (0.1 mM to 10 mM) or combined condition.

5.3 Hypoxia-responsive COFs

It is well-known that hypoxia is a common pathological feature of most solid tumors. By taking advantage of oxygen-deficient property, COFs containing azo groups are easier to be degraded upon azo reductase, which was generated due to the stimulation of aggravated hypoxia, resulting in the release of the encapsulated drugs. For example, Ge *et al.* firstly prepared a hypoxia-responsive COF (TA-COF-P@CT) by incorporating azobenzene groups in the COF skeleton, and further dual-loaded chlorin e6 (Ce6) and tirapazamine (TPZ), where the former is a photodynamic therapeutic agent and the latter is a hypoxia-activated anticancer prodrug.[68] As shown in Fig. 19, the size distribution of the TB-COF-P@CT solution remained unchanged (Fig. 19-II); however, it changed to a triple peak from the original single peak for the TA-COF-P@CT solution (Fig. 19-III) under the same condition. Compared with TB-COF-P@CT, which had no AZO group, the spherical structure of TA-COF-P@CT was destroyed in sodium hydrosulfite ($Na_2S_2O_4$) solution, which worked as a biomimetic azo reductase, strongly supporting the hypoxia-responsive feature of TA-COF-P@CT.

5.4 Protein-responsive COFs

Drug molecules get into the layers of 2D COFs, resulting in their intercalation and storage; however, when they are exposed to the biological environment, which contains serum, the albumin can insert in the COF layers, and followed by the

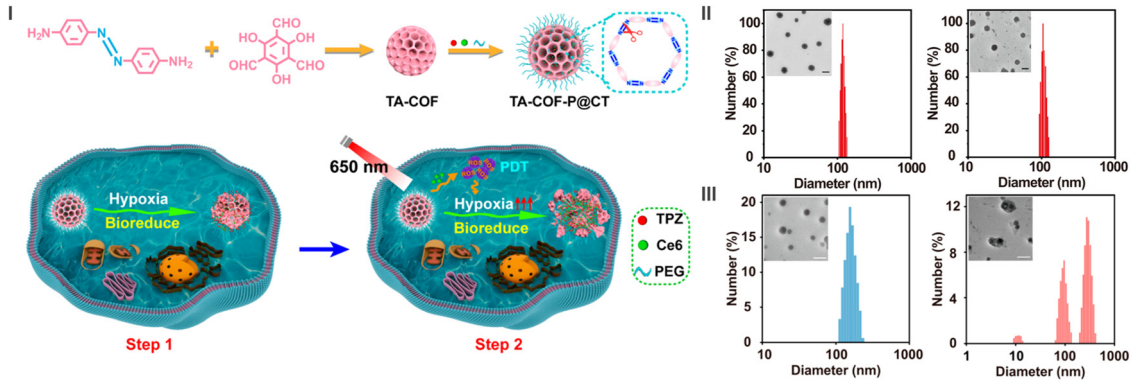

Fig. 19 Hypoxia-responsive COFs. (I) Process for the synthesis of TA-COF-P@CT for light-activated hypoxia-sensitive cancer treatment. Hydrodynamic size distribution and TEM images (inset) of (II) TB-COF-P@CT and (III) TA-COF-P@CT before and after the treatment with $Na_2S_2O_4$. Reproduced from ref. 68 with permission from Nano Letters, Copyright 2021.

exfoliation of the COF layers, ultimately triggering sustained drug release. For example, Subhajit *et al.* synthesized a perylene-based COF (PER@PDA-COF-1), which acted as an effective carrier for the delivery of an anticancer drug mitoxantrone (MXT).[79] The presence of the perylene-like structure could offer a π-electron-rich net layer by layer, and the electrophilic guest molecule MXT could serve as an intercalant between the perylene-comprised 2D layers. Thus, the donor–acceptor interaction between COF and MXT made the whole system strong enough to avoid the premature leakage of MXT from MXT-PER@PDA-COF-1. However, with the additive of albumin, the time-dependent and concentration-dependent intracellular release of MXT was observed, which was attributed to the formation of a protein corona around the exfoliated COF crystallites, followed by the sustained release of MXT from the COF into cancer cells (Fig. 20).

5.5 Photo-responsive COFs

Some COFs with particular cross-linkers can firstly produce $^1O_2$ because of their photo-response, followed by a cascade reaction, which releases the encapsulated drugs due to the destruction of the $^1O_2$-cleavable thioketal linker by the $^1O_2$ generated in the previous step. In conclusion, photo-responsive COFs need to meet two conditions, as follows: (1) a photosensitizer-like linker that can be generated under laser, e.g., porphyrin-based structure and (2) a thioketal-like linker that is sensitive to $^1O_2$. For example, He and co-workers synthesized a nanoscale COF using two linkers including a porphyrin-based monomer tetra(4-hydroxyphenyl)porphine (THPP) and a thioketal-containing monomer, to further load the hypoxia-responsive prodrug banoxantrone (AQ4N) with a high loading (termed AQ4N@$THPP_{TK}$-PEG NPs).[77] Due to the presence of the porphyrin structure, which functioned as a photosensitizer, it was

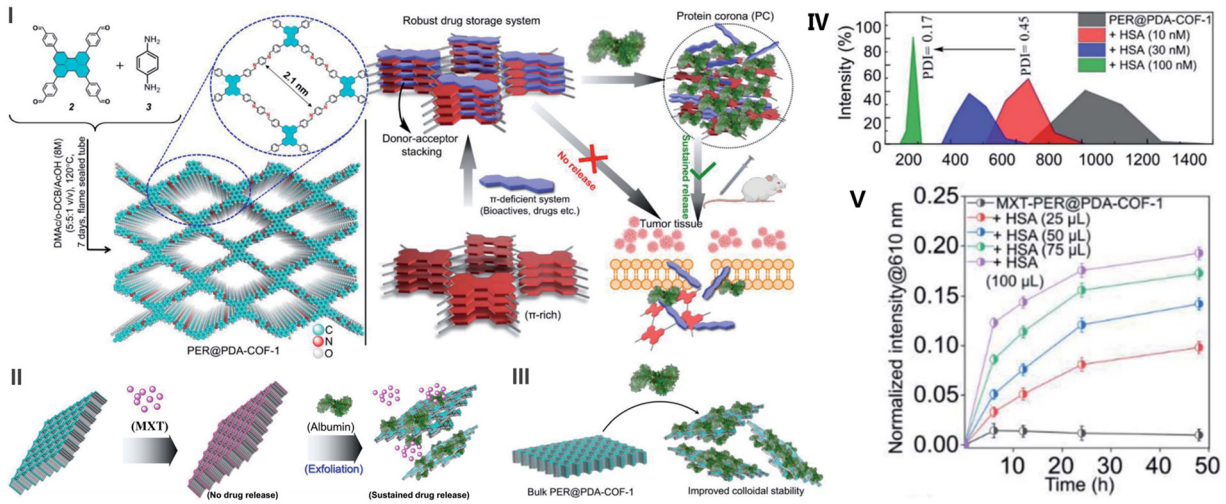

Fig. 20 Protein-responsive COFs. I. Process for the synthesis of PER@PDA-COF-1 and its structure. II. Donor–acceptor based strategy for the loading of bio-actives and albumin-triggered cellular release. III. Schematic representation of albumin-triggered mitoxantrone (MXT) release from the porous host PER@PDA-COF-1. IV. DLS profile of PER@PDA-COF-1 in the presence of different concentrations of albumin. V. Time-dependent drug release profiles of MXT-PER@PDA-COF-1 alone and HAS-MXT-PER@PDA-COF-1 nano-formulations with different albumin concentrations. Reproduced from ref. 79 with permission from Chemical Science, Copyright 2022.

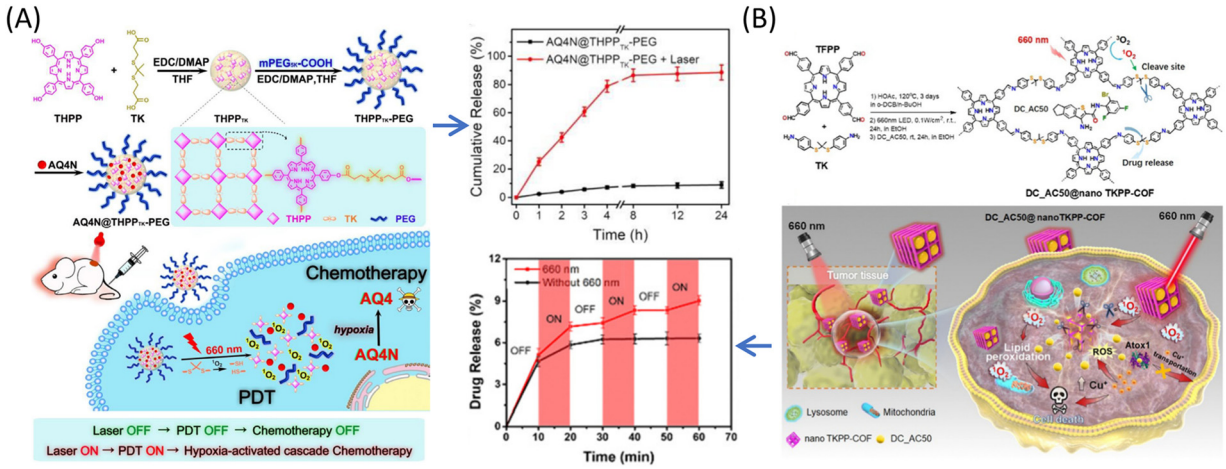

Fig. 21 Photo-responsive COFs. (A) Process for the synthesis of AQ4N@THPPTK-PEG NPs and their combined chemotherapy and photodynamic therapy effects and photo-responsive release behavior under 660 nm laser irradiation. Reproduced from ref. 77 with Acta Biomaterialia, Copyright 2022. (B) Preparation of DC_AC50@nano TKPP-COF and its "on–off" photo-responsive release behavior under 660 nm laser irradiation. Reproduced from ref. 133 with Chemical Communications, Copyright 2023.

easy for AQ4N@THPP$_{TK}$-PEG NPs to generate $^1O_2$. Subsequently, the self-generated $^1O_2$ could break the thioketal linker, and thus allowed the release of AQ4N. In particular, the release of AQ4N showed a laser power density-dependent pattern. When exposed to a 660 nm laser, the release of AQ4N increased to 78.79% within 4 h, compared with only 8.87% after 24 h without a 660 nm laser (Fig. 21(A)). Similarly, Dong's group also reported the preparation of a dithioketal-linked COF for loading of DC_AC50, and the obtained DC_AC50@nano TKPP-COF realized the combination of tumor PDT and chemotherapy.[133] Upon 660 nm laser irradiation, it displayed excellent $^1O_2$ generation ability, and therefore reacted with the dithioketal linkers of the COF skeleton to realize rapid ROS-triggered DC_AC50 release. The release rate was up to 95.2% in 36 h at 200 mW cm^{-2} and 97.7% in 12 h under 600 mW cm^{-2}, whereas only 15.8% in 48 h under the dark condition (Fig. 21(B)).

6. Summary and outlook

The large numbers of studies summarized here illustrated that nanoscale COFs are attracting increasing attention in the field of bioactive delivery because of their unique features including crystallinity and porous structure, efficient loading and controlled release, biocompatibility and biodegradability. Different types of cargos have been embedded in the pores COFs or linked with the COF skeleton using various strategies. The most commonly reported method involves a two-step encapsulation process, comprised of COF synthesis and activation, followed by drug impregnation inside the pores as long as the size of the drugs fits well. However, for the immobilization of biomacromolecules, especially enzymes, more efforts are focused on the one-step encapsulation or hollow encapsulation process. In addition, the covalent binding approach is also a powerful strategy, although it needs a certain amount of bondable active sites for both COFs and cargos. Finally, the coordination bonding strategy is irreplaceable for anchoring metal ions on COFs. To date, several tailored COF-based hybrid composites have been constructed for diverse applications; however, not many have been reported for biomedicine. In this case, there is still room for improving the integration of COFs with other materials.

A variety of stimuli-responsive COFs that can be activated by diverse stimuli including pH, GSH, hypoxia, albumin and light was discussed in this review. For example, imine-based COFs condensed through the Schiff-base reaction have attracted the most attention for pH-responsive release due to the pH-sensitivity of their imine bonds. In addition, by introducing S–S or Se–Se bonds, the spontaneous redox reactions between materials and the microenvironment make GSH-response possible. Similarly, the hypoxia-response is achievable through the introduction of azo bonds in COFs. Furthermore, in the case of 2D COFs for DDS, the layer-by layer exfoliating strategy seems to be a powerful method for controlled release when using a specific protein exfoliating agent.

Based on the current research status, there are still many challenges associated with COFs in bio-applications. Firstly, from the perspective of COF synthesis, more efforts should devoted to obtaining high-quality nanoscale COFs, especially for high crystallinity and porosity. The lack of finite porosity and functionality may result in potential flaws. Secondly, COFs need to be stable enough to carry their entrapped cargos to the biological targets to avoid trigger leakage, causing toxicological effects. Thirdly, there is little or no research on the *in vitro* or *in vivo* pharmacokinetics of COFs. The investigation of possible cumulative and chronic toxicity of monomers degraded from COFs has not been formulated. Fourthly, there is indeed a long way to go before translating basic research results into clinical practice.

In conclusion, the library of COFs that are suitable for the integration and delivery of cargos is growing as research proceeds, and it will continue to be an attractive and

challenging research field. We hope that this review article will inspire follow-up studies on COFs for the integration, delivery and controlled release of bioactives.

Conflicts of interest

The authors declare no potential conflicts of interest.

Acknowledgements

This work was financially supported by the National Natural Science Foundation of China (T2222021, 32025021, 31971292, and 32011530115), the Key R&D Program of Zhejiang Province (2020C03110), the Science & Technology Bureau of Ningbo City (2020Z094, 2021Z072) and Excellent Member of Youth Innovation Promotion Association Foundation of CAS (Y2021079). The authors also acknowledged Shanghai Synchrotron Radiation Facility at BL19U2 used for small-angle X-ray scattering.

References

1 E. Ploetz, H. Engelke, U. Lächelt and S. Wuttke, *Adv. Funct. Mater.*, 2020, **30**, 1909062.
2 H. S. Sasmal, A. Kumar Mahato, P. Majumder and R. Banerjee, *J. Am. Chem. Soc.*, 2022, **144**, 11482–11498.
3 W. Zhang, L. Chen, S. Dai, C. Zhao, C. Ma, L. Wei, M. Zhu, S. Y. Chong, H. Yang, L. Liu, Y. Bai, M. Yu, Y. Xu, X. W. Zhu, Q. Zhu, S. An, R. S. Sprick, M. A. Little, X. Wu, S. Jiang, Y. Wu, Y. B. Zhang, H. Tian, W. H. Zhu and A. I. Cooper, *Nature*, 2022, **604**, 72–79.
4 Y. G. Hui, Z. Zhe, Y. C. Cong, S. X. Song and W. Yong, *Chin. J. Polym. Sci.*, 2022, **40**, 338–344.
5 A. M. Vargason, A. C. Anselmo and S. Mitragotri, *Nat. Biomed. Eng.*, 2021, **5**, 951–967.
6 Z. Zhao, W. Wang, C. Li, Y. Zhang, T. Yu, R. Wu, J. Zhao, Z. Liu, J. Liu and H. Yu, *Adv. Funct. Mater.*, 2019, **29**, 1905013.
7 S. Mallakpour, E. Nikkhoo and C. M. Hussain, *Coord. Chem. Rev.*, 2022, **451**, 214262.
8 Y. Cao, X. Ge, X. Zhu, Y. Han, P. Wang, O. U. Akakuru, A. Wu and J. Li, *Adv. Sci.*, 2023, **10**, e2300545.
9 Y. Hu, L. Dai, D. Liu, W. Du and Y. Wang, *Renewable Sustainable Energy Rev.*, 2018, **91**, 793–801.
10 Y. Zhao, Y. Liang, D. Wu, H. Tian, T. Xia, W. Wang, W. Xie, X. M. Hu, X. Tian and Q. Chen, *Small*, 2022, e2107750.
11 S. Maiti, A. R. Chowdhury and A. K. Das, *ChemNanoMat*, 2019, **6**, 99–106.
12 L. Zhang, R. Bu, X.-Y. Liu, P.-F. Mu and E.-Q. Gao, *Green Chem.*, 2021, **23**, 7620–7629.
13 L.-G. Ding, B.-J. Yao, F. Li, S.-C. Shi, N. Huang, H.-B. Yin, Q. Guan and Y.-B. Dong, *J. Mater. Chem. A*, 2019, **7**, 4689–4698.
14 O. F. Altundal, C. Altintas and S. Keskin, *J. Mater. Chem. A*, 2020, **8**, 14609–14623.
15 P. Das and S. K. Mandal, *Chem. Mater.*, 2019, **31**, 1584–1596.
16 H. Zhang and H. Li, *J. Mater. Chem. C*, 2022, **10**, 13834–13843.
17 X. F. Liu, H. Chen, R. Wang, S. Q. Zang and T. C. W. Mak, *Small*, 2020, **16**, e2002932.
18 Z. Xie, B. Wang, Z. Yang, X. Yang, X. Yu, G. Xing, Y. Zhang and L. Chen, *Angew. Chem., Int. Ed.*, 2019, **58**, 15742–15746.
19 Y. Shi, J. Yang, F. Gao and Q. Zhang, *ACS Nano*, 2023, **17**, 1879–1905.
20 A. Mal, H. Ding, M. Li, W. Li and C. Wang, *ACS Appl. Nano Mater.*, 2022, **5**, 13972–13984.
21 X. Wang, D. A. Lewis, G. Wang, T. Meng, S. Zhou, Y. Zhu, D. Hu, S. Gao and G. Zhang, *Adv. Ther.*, 2022, **5**, 2200053.
22 L. Wang, H. Xie, Y. Lin, M. Wang, L. Sha, X. Yu, J. Yang, J. Zhao and G. Li, *Biosens. Bioelectron.*, 2022, **217**, 114668.
23 Y. Zhang, X. Xu, Q. Liao, Q. Wang, Q. Han, P. Chen and K. Xi, *J. Mater. Chem. B*, 2022, **10**, 3285–3292.
24 L. Zhang, Y. Xiao, Q. C. Yang, L. L. Yang, S. C. Wan, S. Wang, L. Zhang, H. Deng and Z. J. Sun, *Adv. Funct. Mater.*, 2022, **32**, 2201542.
25 M. Wang, M. Ballabio, M. Wang, H. H. Lin, B. P. Biswal, X. Han, S. Paasch, E. Brunner, P. Liu, M. Chen, M. Bonn, T. Heine, S. Zhou, E. Canovas, R. Dong and X. Feng, *J. Am. Chem. Soc.*, 2019, **141**, 16810–16816.
26 M. Siebels, C. Schlüsener, J. Thomas, Y.-X. Xiao, X.-Y. Yang and C. Janiak, *J. Mater. Chem. A*, 2019, **7**, 11934–11943.
27 P. Kuhn, M. Antonietti and A. Thomas, *Angew. Chem., Int. Ed.*, 2008, **47**, 3450–3453.
28 B. Diaz de Grenu, J. Torres, J. Garcia-Gonzalez, S. Munoz-Pina, R. de Los Reyes, A. M. Costero, P. Amoros and J. V. Ros-Lis, *ChemSusChem*, 2021, **14**, 208–233.
29 W. Zhao, P. Yan, H. Yang, M. Bahri, A. M. James, H. Chen, L. Liu, B. Li, Z. Pang, R. Clowes, N. D. Browning, J. W. Ward, Y. Wu and A. I. Cooper, *Nat., Synth.*, 2022, **1**, 87–95.
30 D. Wang, L. Lin, T. Li, M. Meng, K. Hao, Z. Guo, J. Chen, H. Tian and X. Chen, *Adv. Mater.*, 2022, e2205924.
31 R. Xia, C. Li, X. Yuan, Q. Wu, B. Jiang and Z. Xie, *ACS Appl. Mater. Interfaces*, 2022, **14**, 19129–19138.
32 X. Shi, L. Yi and H. Deng, *Sci. China: Chem.*, 2022, **65**, 1315–1320.
33 D. Zhu, Z. Zhang, L. B. Alemany, Y. Li, N. Nnorom, M. Barnes, S. Khalil, M. M. Rahman, P. M. Ajayan and R. Verduzco, *Chem. Mater.*, 2021, **33**, 3394–3400.
34 X. Li, T. Goto, K. Nomura, M. Zhu, T. Sekino and Y. Osakada, *Appl. Surf. Sci.*, 2020, **513**, 145720.
35 S. Kandambeth, K. Dey and R. Banerjee, *J. Am. Chem. Soc.*, 2019, **141**, 1807–1822.
36 X. Wang, P. She and Q. Zhang, *Smart Mater.*, 2021, **2**, 299–325.
37 J. Yuan, X. You, N. A. Khan, R. Li, R. Zhang, J. Shen, L. Cao, M. Long, Y. Liu, Z. Xu, H. Wu and Z. Jiang, *Nat. Commun.*, 2022, **13**, 3826.
38 S. Das, T. Sekine, H. Mabuchi, T. Irie, J. Sakai, Y. Zhao, Q. Fang and Y. Negishi, *ACS Appl. Mater. Interfaces*, 2022, **14**, 48045–48051.
39 S. K. Das, S. Roy, A. Das, A. Chowdhury, N. Chatterjee and A. Bhaumik, *Nanoscale Adv.*, 2022, **4**, 2313–2320.

40 Z. Han, Y. Qian, X. Gao, D. Yang, Y. Cai, Y. Chen, J. Jin and Z. Yang, *Colloids Surf., B*, 2023, **222**, 113094.
41 Q. Guan, L. L. Zhou and Y. B. Dong, *Adv. Ther.*, 2021, **5**, 2100177.
42 S. Liu, C. Hu, Y. Liu, X. Zhao, M. Pang and J. Lin, *Chemistry*, 2019, **25**, 4315–4319.
43 Y. Zou, P. Wang, A. Zhang, Z. Qin, Y. Li, Y. Xianyu and H. Zhang, *ACS Appl. Mater. Interfaces*, 2022, **14**, 8680–8692.
44 H. Chao, Z. Zhou, W. He, M. Li, X. Yuan, P. Su, J. Song and Y. Yang, *ACS Appl. Mater. Interfaces*, 2022, **14**, 20641–20651.
45 C. Du, W. Na, M. Shao, S. Shang, Y. Liu and J. Chen, *Chem. Mater.*, 2023, **35**, 1395–1403.
46 M. Li, S. Qiao, Y. Zheng, Y. H. Andaloussi, X. Li, Z. Zhang, A. Li, P. Cheng, S. Ma and Y. Chen, *J. Am. Chem. Soc.*, 2020, **142**, 6675–6681.
47 S. Liu, K. Dou, B. Liu, M. Pang, P. Ma and J. Lin, *Angew. Chem., Int. Ed.*, 2023, **135**, e202301831.
48 S. Mitra, H. S. Sasmal, T. Kundu, S. Kandambeth, K. Illath, D. Diaz Diaz and R. Banerjee, *J. Am. Chem. Soc.*, 2017, **139**, 4513–4520.
49 Z. Mi, P. Yang, R. Wang, J. Unruangsri, W. Yang, C. Wang and J. Guo, *J. Am. Chem. Soc.*, 2019, **141**, 14433–14442.
50 Q. Guan, D. D. Fu, Y. A. Li, X. M. Kong, Z. Y. Wei, W. Y. Li, S. J. Zhang and Y. B. Dong, *iScience*, 2019, **14**, 180–198.
51 L. L. Zhou, Q. Guan, W. Y. Li, Z. Zhang, Y. A. Li and Y. B. Dong, *Small*, 2021, **17**, e2101368.
52 P. Gao, T. Zheng, B. Cui, X. Liu, W. Pan, N. Li and B. Tang, *Chem. Commun.*, 2021, **57**, 13309–13312.
53 S. Liu, Y. Zhou, C. Hu, L. Cai and M. Pang, *ACS Appl. Mater. Interfaces*, 2020, **12**, 43456–43465.
54 L. Zhang, Q. C. Yang, S. Wang, Y. Xiao, S. C. Wan, H. Deng and Z. J. Sun, *Adv. Mater.*, 2021, **34**, e2108174.
55 Q. Fang, J. Wang, S. Gu, R. B. Kaspar, Z. Zhuang, J. Zheng, H. Guo, S. Qiu and Y. Yan, *J. Am. Chem. Soc.*, 2015, **137**, 8352–8355.
56 L. Bai, S. Z. Phua, W. Q. Lim, A. Jana, Z. Luo, H. P. Tham, L. Zhao, Q. Gao and Y. Zhao, *Chem. Commun.*, 2016, **52**, 4128–4131.
57 Y. Luo, J. Liu, Y. Liu and Y. Lyu, *J. Polym. Sci., Part A: Polym. Chem.*, 2017, **55**, 2594–2600.
58 G. Zhang, X. Li, Q. Liao, Y. Liu, K. Xi, W. Huang and X. Jia, *Nat. Commun.*, 2018, **9**, 2785.
59 Q. Guan, L. L. Zhou, Y. A. Li, W. Y. Li, S. Wang, C. Song and Y. B. Dong, *ACS Nano*, 2019, **13**, 13304–13316.
60 N. Mokhtari, S. Taymouri, M. Mirian and M. Dinari, *J. Mol. Liq.*, 2019, **297**, 111898.
61 K. Wang, Z. Zhang, L. Lin, K. Hao, J. Chen, H. Tian and X. Chen, *ACS Appl. Mater. Interfaces*, 2019, **11**, 39503–39512.
62 L. Akyuz, *Microporous Mesoporous Mater.*, 2020, **294**, 109850.
63 Y. Jia, L. Zhang, B. He, Y. Lin, J. Wang and M. Li, *Mater. Sci. Eng., C*, 2020, **117**, 111243.
64 S. Liu, J. Yang, R. Guo, L. Deng, A. Dong and J. Zhang, *Macromol. Rapid Commun.*, 2020, **41**, e1900570.
65 B. Wang, X. Liu, P. Gong, X. Ge, Z. Liu and J. You, *Chem. Commun.*, 2020, **56**, 519–522.
66 C. Wang, H. Liu, S. Liu, Z. Wang and J. Zhang, *Front. Chem.*, 2020, **8**, 488.
67 S. B. Wang, Z. X. Chen, F. Gao, C. Zhang, M. Z. Zou, J. J. Ye, X. Zeng and X. Z. Zhang, *Biomaterials*, 2020, **234**, 119772.
68 L. Ge, C. Qiao, Y. Tang, X. Zhang and X. Jiang, *Nano Lett.*, 2021, **21**, 3218–3224.
69 Q. Sun, K. Tang, L. Song, Y. Li, W. Pan, N. Li and B. Tang, *Biomater. Sci.*, 2021, **9**, 7977–7983.
70 R. Anbazhagan, R. Krishnamoorthi, S. Kumaresan and H. C. Tsai, *Mater. Sci. Eng., C*, 2021, **120**, 111704.
71 W. Zhao, C. Yu, J. Zhao, F. Chen, X. Guan, H. Li, B. Tang, G. Yu, V. Valtchev, Y. Yan, S. Qiu and Q. Fang, *Small*, 2021, **17**, e2102630.
72 W. Wang, Y. Song, J. Chen, Y. Yang, J. Wang, Y. Song, J. Ni, M. Tang, J. Zhao, Y. Sun, T. Sun and J. Peng, *J. Mater. Chem. B*, 2022, **10**, 1128–1135.
73 L. Liao, Z. Zhang, X. Guan, H. Li, Y. Liu, M. Zhang, B. Tang, V. Valtchev, Y. Yan, S. Qiu, X. Yao and Q. Fang, *Chin. J. Chem.*, 2022, **40**, 2081–2088.
74 Y. Wang, X. Sun and Y. Wang, *RSC Adv.*, 2022, **12**, 16046–16050.
75 B. Ma, Y. Xu, F. Hu, L. Zhai, Y. Huang, H. Qiao, J. Xiong, D. Yang, Z. Ni, X. Zheng and L. Mi, *RSC Adv.*, 2022, **12**, 31276–31281.
76 C. Huang, S. Zhou, C. Chen, X. Wang, R. Ding, Y. Xu, Z. Cheng, Z. Ye, L. Sun, Z. J. Wang, D. Hu, X. Jia, G. Zhang and S. Gao, *Small*, 2022, **18**, e2205062.
77 H. He, L. Du, H. Xue, J. Wu and X. Shuai, *Acta Biomater.*, 2022, **149**, 297–306.
78 D. Dutta, J. Wang, X. Li, Q. Zhou and Z. Ge, *Small*, 2022, **18**, e2202369.
79 S. Bhunia, P. Saha, P. Moitra, M. A. Addicoat and S. Bhattacharya, *Chem. Sci.*, 2022, **13**, 7920–7932.
80 H. Lou, L. Chu, W. Zhou, J. Dou, X. Teng, W. Tan and B. Zhou, *J. Mater. Chem. B*, 2022, **10**, 7955–7966.
81 L. Zhang, Y. Jia, H. Hao, M. Wang and J. Wang, *Microporous Mesoporous Mater.*, 2022, **344**, 112198.
82 K. Yao, X. Liang, G. Zhang, Y. Rong, Q. Zhang, Q. Liao, H. Zhang, K. Xi and J. Wang, *Polymers*, 2022, **14**, 3265.
83 Q. Du, J. Zou, Z. Huang, S. Li, L. Tan, X. Ren, G. Yin, Y. Zheng and X. Meng, *Chin. Chem. Lett.*, 2022, **34**, 107763.
84 L. Yao, Z. Zhou, S. Wang, Q. Zou, H.-X. Wang, L.-X. Ma, S. Wang and X. Zhang, *Chem. Sci.*, 2022, **13**, 5902–5912.
85 Y. Zhao, S. Das, T. Sekine, H. Mabuchi, T. Irie, J. Sakai, D. Wen, W. Zhu, T. Ben and Y. Negishi, *Angew. Chem., Int. Ed.*, 2023, e202300172.
86 W. Y. Li, J. J. Wan, J. L. Kan, B. Wang, T. Song, Q. Guan, L. L. Zhou, Y. A. Li and Y. B. Dong, *Chem. Sci.*, 2023, **14**, 1453–1460.
87 S. Zhang, S. Xia, L. Chen, Y. Chen and J. Zhou, *Adv. Sci.*, 2023, **10**, e2206009.
88 S. Kandambeth, V. Venkatesh, D. B. Shinde, S. Kumari, A. Halder, S. Verma and R. Banerjee, *Nat. Commun.*, 2015, **6**, 6786.
89 S. Zhang, Y. Zheng, H. An, B. Aguila, C. X. Yang, Y. Dong, W. Xie, P. Cheng, Z. Zhang, Y. Chen and S. Ma, *Angew. Chem., Int. Ed.*, 2018, **57**, 16754–16759.

90 Q. Sun, C. W. Fu, B. Aguila, J. Perman, S. Wang, H. Y. Huang, F. S. Xiao and S. Ma, *J. Am. Chem. Soc.*, 2018, **140**, 984–992.
91 A. Samui, Happy and S. K. Sahu, *Microporous Mesoporous Mater.*, 2020, **291**, 109700.
92 P. Gao, M. Wang, Y. Chen, W. Pan, P. Zhou, X. Wan, N. Li and B. Tang, *Chem. Sci.*, 2020, **11**, 6882–6888.
93 Y. Zhou, S. Liu, C. Hu, L. Cai and M. Pang, *J. Mater. Chem. B*, 2020, **8**, 5451–5459.
94 G. Zhang, Y. Ji, X. Li, X. Wang, M. Song, H. Gou, S. Gao and X. Jia, *Adv. Healthcare Mater.*, 2020, **9**, e2000221.
95 F. Benyettou, N. Kaddour, T. Prakasam, G. Das, S. K. Sharma, S. A. Thomas, F. Bekhti-Sari, J. Whelan, M. A. Alkhalifah, M. Khair, H. Traboulsi, R. Pasricha, R. Jagannathan, N. Mokhtari-Soulimane, F. Gandara and A. Trabolsi, *Chem. Sci.*, 2021, **12**, 6037–6047.
96 X. Wan, H. Zhang, W. Pan, N. Li and B. Tang, *Chem. Commun.*, 2021, **57**, 5402–5405.
97 P. Gao, R. Wei, Y. Chen, X. Liu, J. Zhang, W. Pan, N. Li and B. Tang, *Anal. Chem.*, 2021, **93**, 13734–13741.
98 P. Gao, K. Tang, R. Lou, X. Liu, R. Wei, N. Li and B. Tang, *Anal. Chem.*, 2021, **93**, 12096–12102.
99 Y. Cao, J. Zhang, L. Wang, M. Cen, W. Peng, Y. Li, F. Zhang, J. Tan and X. Fan, *ACS Appl. Nano Mater.*, 2021, **4**, 4948–4955.
100 C. Xing, P. Mei, Z. Mu, B. Li, X. Feng, Y. Zhang and B. Wang, *Angew. Chem., Int. Ed.*, 2022, **61**, e202201378.
101 J. Lu, Y. Han, K. Wang, Y. Zhang, J. Li, Y. Xu, L. Sun, J. Yang and G. Li, *Anal. Chem.*, 2022, **94**, 15139–15145.
102 T. Li, D. Deng, D. Tan, S. Chen, Y. Ji and R. Li, *Anal. Bioanal. Chem.*, 2022, **414**, 6247–6257.
103 J. Lu, M. Wang, Y. Han, Y. Deng, Y. Zeng, C. Li, J. Yang and G. Li, *Anal. Chem.*, 2022, **94**, 5055–5061.
104 Y. Lin, Y. Deng, M. Wang, T. Zhou, L. Wang, J. Ma and J. Yang, *Talanta*, 2023, **253**, 124043.
105 Q. Ren, H. Chen, Y. Chen, Z. Song, S. Ouyang, S. Lian, J. Tao, Y. Song and P. Zhao, *ACS Appl. Mater. Interfaces*, 2023, **15**, 4947–4958.
106 C. Zhong, G. Li, W. Tian, D. Ouyang, Y. Ji, Z. Cai and Z. Lin, *ACS Appl. Mater. Interfaces*, 2023, **15**, 10158–10165.
107 Y. Zhang, C. Xing, Z. Mu, Z. Niu, X. Feng, Y. Zhang and B. Wang, *J. Am. Chem. Soc.*, 2023, **145**, 13469–13475.
108 B. Sun, F. Wu, X. Wang, Q. Song, Z. Ye, M. Mohammadniaei, M. Zhang, X. Chu, S. Xi, N. Zhou, W. Wang, C. Yao and J. Shen, *Small*, 2022, **18**, e2200895.
109 S. Gan, X. Tong, Y. Zhang, J. Wu, Y. Hu and A. Yuan, *Adv. Funct. Mater.*, 2019, **29**, 1902757.
110 K. Hao, Z. Guo, L. Lin, P. Sun, Y. Li, H. Tian and X. Chen, *Sci. China: Chem.*, 2021, **64**, 1235–1241.
111 J. Chen, Y. Wang, Y. Yu, J. Wang, J. Liu, H. Ihara and H. Qiu, *Exploration*, 2023, **3**, 20220144.
112 M. Wang, Y. Pan, S. Wu, Z. Sun, L. Wang, J. Yang, Y. Yin and G. Li, *Biosens. Bioelectron.*, 2020, **169**, 112638.
113 P. Gao, R. Wei, Y. Chen, X. Li, W. Pan, N. Li and B. Tang, *Biomaterials*, 2023, **297**, 122109.
114 X. Liu, M. Hu, M. Wang, Y. Song, N. Zhou, L. He and Z. Zhang, *Biosens. Bioelectron.*, 2019, **123**, 59–68.
115 M. Xu, K. Chen, L. Zhu, S. Zhang, M. Wang, L. He, Z. Zhang and M. Du, *Langmuir*, 2021, **37**, 13479–13492.
116 Y. Li, Z. Liu, W. Lu, M. Zhao, H. Xiao, T. Hu, J. Ma, Z. Zheng, J. Jia and H. Wu, *Analyst*, 2021, **146**, 979–988.
117 S. Li, Z. Chen, L. Tan, Q. Wu, X. Ren, C. Fu, M. Niu, H. Li and X. Meng, *Biomaterials*, 2022, **283**, 121472.
118 P. Wang, M. Li, F. Zhou, Y. Yang, X. Yin, X. Zhang and G. Song, *Chem. Commun.*, 2022, **58**, 11107–11110.
119 R. Yuan, Z. Yan and H. He, *Appl. Surf. Sci.*, 2022, **573**, 151556.
120 Y. Zhou, S. Jing, S. Liu, X. Shen, L. Cai, C. Zhu, Y. Zhao and M. Pang, *J. Nanobiotechnol.*, 2022, **20**, 188.
121 H. Liang, G. Ning, L. Wang, C. Li, J. Zheng, J. Zeng, H. Zhao and C.-P. Li, *ACS Appl. Nano Mater.*, 2021, **4**, 4593–4601.
122 K. Zhao, P. Gong, J. Huang, Y. Huang, D. Wang, J. Peng, D. Shen, X. Zheng, J. You and Z. Liu, *Microporous Mesoporous Mater.*, 2021, **311**, 110713.
123 L. Wang, W. Gao, S. Ng and M. Pumera, *Anal. Chem.*, 2021, **93**, 5277–5283.
124 D. Liang, X. Zhang, Y. Wang, T. Huo, M. Qian, Y. Xie, W. Li, Y. Yu, W. Shi, Q. Liu, J. Zhu, C. Luo, Z. Cao and R. Huang, *Bioact. Mater.*, 2022, **14**, 145–151.
125 H. Li, B. Kou, Y. Yuan, Y. Chai and R. Yuan, *Biosens. Bioelectron.*, 2022, **197**, 113758.
126 C. Fu, T. Lu, X. Dai, P. Ding, Y. Xiong, J. Ge and X. Li, *ACS Appl. Mater. Interfaces*, 2023, **15**, 6859–6867.
127 Z. Lu, S. Bai, Y. Jiang, S. Wu, D. Xu, Y. Chen, Y. Lan, Y. An, J. Mao, X. Liu and G. Liu, *Adv. Funct. Mater.*, 2022, **32**, 2207749.
128 T. Huo, X. Zhang, M. Qian, H. Nie, D. Liang, C. Lin, Y. Yang, W. Guo, U. Lachelt and R. Huang, *Adv. Sci.*, 2022, **9**, e2200608.
129 S. He, L. Wu, H. Sun, D. Wu, C. Wang, X. Ren, Q. Shao, P. York, J. Tong, J. Zhu, Z. Li and J. Zhang, *ACS Appl. Mater. Interfaces*, 2022, **14**, 38421–38435.
130 M. C. Wang, J. X. Guo, L. J. Chen and X. Zhao, *Biomater. Sci.*, 2023, **11**, 1776–1784.
131 S. Wang, Y. Pang, S. Hu, J. Lv, Y. Lin and M. Li, *Chem. Eng. J.*, 2023, **451**, 138864.
132 J. Feng, W.-X. Ren, F. Kong, C. Zhang and Y.-B. Dong, *Sci. China Mater.*, 2021, **65**, 1122–1133.
133 W. Y. Li, J. L. Kan, J. J. Wan, Y. A. Li, T. Song, B. Wang, Q. Guan, L. L. Zhou and Y. B. Dong, *Chem. Commun.*, 2023, **59**, 5423–5426.